Blind Parameters Estimation by Exploiting Cyclostationary Features in Wavelet Domain

Student Name: Sushant Kumar

IIIT-D-MTech-ECE-14-16
Thu 28, 2016

Indraprastha Institute of Information Technology
New Delhi

Thesis Committee
Dr. Vivek Ashok Bohara (Chair)
Dr. Sumit J Darak (Chair)
Dr. Anubha Gupta
Dr. A.V. Subramanyam

Submitted in partial fulfillment of the requirements
for the Degree of M.Tech. in Electronics and Communication

Keywords: Continuous wavelet transform, cyclostationary feature detection, denoising, blind wireless receiver, symbol rate estimation, modulation classification, carrier frequency estimation, complexity analysis, histogram

Certificate

This is to certify that the thesis titled **"Blind Parameters Estimation by Exploiting Cyclostationary Features in Wavelet Domain"** submitted by **Sushant Kumar** for the partial fulfillment of the requirements for the degree of *Master of Technology* in *Electronics and Communication & Engineering* is a record of the bonafide work carried out by her / him under my / our guidance and supervision in the Security and Privacy group at Indraprastha Institute of Information Technology, Delhi. This work has not been submitted anywhere else for the reward of any other degree.

Dr. Vivek Ashok Bohara
Indraprastha Institute of Information Technology, New Delhi

Dr. Sumit J Darak
Indraprastha Institute of Information Technology, New Delhi

Abstract

In dynamic environment, multi-standard wireless communication receivers capable of estimating the various parameters of any unknown modulated signal are desired. These parameters include symbol rate, modulation type, carrier frequency etc. For identifying the modulation type, symbol rate estimation is primary step while carrier frequency estimation is useful when there is relative motion between transmitter and receiver. Accurate estimation of these parameters is the objective of the work presented in this thesis.

The first contribution of the thesis is symbol rate estimation and modulation classifier. The proposed method exploits cyclostationary features of the received signal in wavelet domain. Simulation results for AWGN and Rayleigh fading channel shows the superiority of the proposed approach over existing approaches especially at low SNRs. The proposed method then extended to the automatic modulation classification and estimation of carrier frequency. At the end, detailed complexity analysis based on total number of gate counts is presented.

Acknowledgments

Towards the end of my Master degree, I would like to pay my heartily gratitude to several individuals who contributed in many ways. First of all, I would like to express my deep gratitude to my thesis supervisor, Dr. Vivek Ashok Bohara and Dr. Sumit J Darak for their support, guidance and motivation all along the way. I feel extremely fortunate to work with them. They has been great sources of inspiration to me and I thank them from the bottom of my heart. I would like to thank Dr. Pankaj Jalote and all my professors at IIITD for providing such a wonderful environment to work. I would like to express my gratitude towards my family for their kind co-operation and encouragement which give me a source of motivation. Last but not the least, I want to thank my friends for all thoughtful discussions we had, which prompted me to think beyond the obvious.

Contents

List of Figures

List of Tables

List of abbrevation

ALRT	average likelihood ratio tests.
AMC	automatic modulation classifier
AWGN	additive white Gaussian noise
BPSK	binary phase shift keying
BWR	blind wireless receiver
CFD	cyclostationary feature detection
CWT	continuous wavelet transform
FT	fourier transform
FT	quadrature phase shift keying
GLRT	generalized likelihood ratio tests
HLRT	hybrid likelihood ratio tests
HOMs	high order moments
KNN	k-nearest neighbor
PAM	pulse amplitude modulation
QAM	quadrature amplitude modulation
SNR	signal to noise ratio
STFT	short time fourier transform
SVM	support vector machine
WT	wavelet transform

[**?**]

Chapter 1

Introduction

1.1 Motivation and objective

In the next-generation wireless communication, spectrum crisis is going to be one of the major problem. However, there is shortage of spectrum, still huge amount of spectrum is wasted just in transmitting some redundant data and training sequences. Hence, immense amount of the spectrum allocated to user is not efficiently utilized by the user. One way to increase bandwidth efficiency is to use blind wireless receiver (BWR) [1,2] [3–8] [9] [10], where parameters (carrier frequency, symbol rate, modulation type, timing offset, phase offset) can be estimated at receiver by utilizing some properties of received signal. In this way, redundant data and training sequences are not needed at the receiver and thus, BWR releases unused spectrum for the other user to reuse it. For example, Automatic Modulation Classifier (AMC) is an important for the receiver that has no, or limited, knowledge of signal received as it is intermediate step between signal detection and demodulation. In modern communication AMC is widely used in adaptive modulation, where the modulation scheme is switched dynamically with the change in channel. It means modulation type of transmitted signal can change with change in state of channel, like whenever channel is clean higher level modulation can be transmitted, and low level modulation scheme can be transmitted in noisy channel. Information about modulation type of transmitted signal is must for receiver in order to demodulate at receiver side to extract the original transmitted message. One way to do this is by sending a pilot signal along with the original message to inform the receiver about the modulation type. However, the above technique is applicable but it comes at the cost of loss of bandwidth efficiency and reduction in data throughput due to periodically sending pilot signals that carry no data, especially for those having small data blocks.The blind wireless receiver can remove this drawback where some properties of the received signal can be used to identify modulation. The BWR can act as a universal receiver as in it signals of different standards can be received by single receiver. Unlike cognitive radio, where secondary users can use unused spectrum of primary users, in BWR excess spectrum can be used by primary users.

In BWR, some blind estimation algorithms can be applied to estimate unknown parameters

like carrier frequency, symbol rate, modulation type, phase offset etc. Various algorithms have been proposed for parameter estimations using wavelet transform, cyclostationarity, filter bank, cyclic correlation, and inverse fourier transform [3–8] [9] [10], higher order cumulant, maximum likelihood algorithm etc. Details of these algorithms are discussed in subsequent chapters.

In this thesis, we alleviate the drawbacks of conventional algorithms by proposing a new method to blindly estimate the symbol rate of a received signal. The proposed algorithm exploits excellent localization property of wavelet transform along with superiority of cyclostationary feature detection in low SNR environment. Simulation and gate count complexity results validate the superiority of the proposed algorithm over other algorithms proposed in literature. Then a simple technique is proposed using histogram of received signal to automatically identify modulation type. The proposed scheme is tested for BPSK, QPSK, 8-PSK, 4-PAM, and 16-QAM modulation types in Additive White Gaussian Noise (AWGN) and flat fading environment. These modulation scheme are widely used in modern digital communication. For example, commonly QAM is used in digital microwave communication and telephone line modem.

1.2 Contribution

We have proposed a symbol rate estimator which exploits excellent localization property of wavelet transform along with superiority of cyclostationary feature detection in low SNR environment. Simulation and gate count complexity results validate the superiority of the proposed algorithm over other algorithms proposed in literature.

- Sushant Kumar, Sumit J Darak and Vivek Ashok Bohara, "Blind Symbol Rate Estimation by Exploiting Cyclostationary Features in Wavelet Domain" accepted in *International Conference on Advances in Computing, Communications and Informatics (ICACCI), Jaipur, India, Sept. 2016.*

We have proposed a simple technique using histogram of received signal to automatically identify modulation type. Simulation results show the superiority of the proposed algorithm over other algorithms proposed in literature.

We have proposed a carrier frequency estimator which also exploits excellent localization property of wavelet transform along with superiority of cyclostationary feature detection in low SNR environment.

1.3 Terminologies

1.3.1 Wavelet denoising

Denoising is a method of reducing the noise from received signal which has been contaminated due to AWGN. Conventionally, fast Fourier transform has been preferred for denoising operation

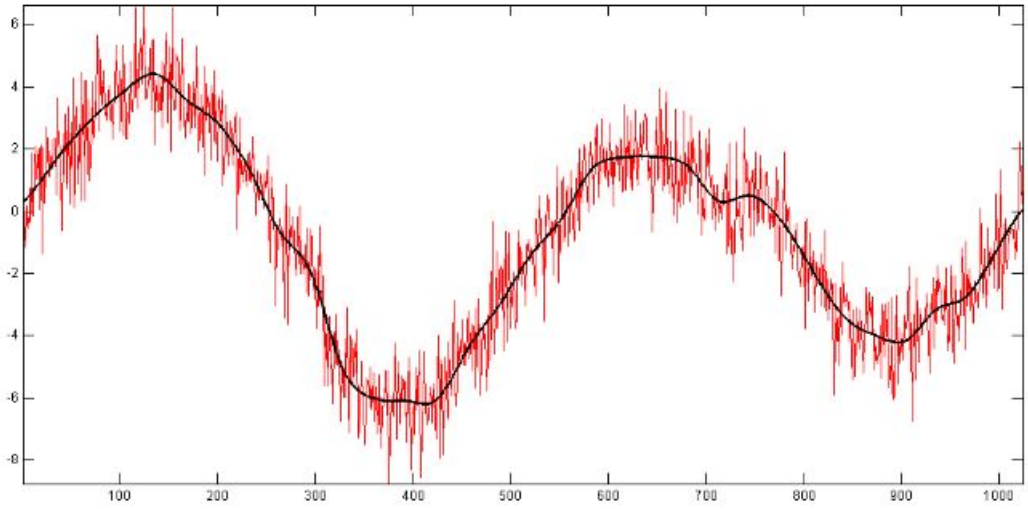

Figure 1.1: Noisy sine and its denoised version (solid line)

[8]. However, it leads to loss of high frequency component in the received signal. Example of a noisy signal and its denoised version is shown in Fig. 1.1. Denoising process can be process in three steps:

- Decompose
- Threshold details coefficient
- Reconstruct

Decompose

In first step wavelet decomposition of level N is computed. It is a hierarchical scheme in which inner product is calculated using set of high pass filters and low pass filters followed by decimation as shown in Fig. 1.2. As a result, signal is decomposed into different scales which are considered as different frequency bands. Coefficients of low-pass and high-pass filter coefficients can be determined by mother wavelet in use. The output of low-pass filter is called approximation coefficients and output of high-pass is called detailed coefficients. Number of levels is determined by the user depending upon characters of the signal to be analyzed. Generally it taken to be 3-5.

Threshold details coefficient

Thresholding is applied on detail coefficients as it contains high-pass coefficients and noise also contain high-pass components. Then, soft thresholding is applied on all the detailed coefficients where the threshold (T_i) for i^{th} level is related to variance, σ_i^2 and is given by,

$$T_i = \gamma_i \sigma_i, \tag{1.1}$$

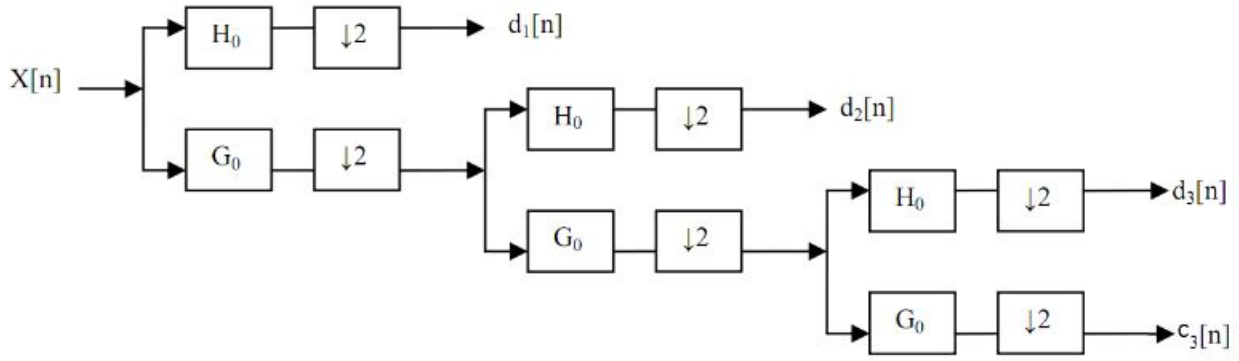

Figure 1.2: 3-level decomposition of a signal. H_0 is an HPF and G_0 is a LPF. $c_j(n)$ is approximation coefficient and $d_j(n)$ is detail coefficient

where

γ_i is a level factor.

Level factor which depends on the distribution of details coefficients, and is equal to 2.5 for a normally distributed data. Distribution of noise is shown in Fig. 1.3 through histogram plot of noise. It is clear from the Fig. 1.3 that most of the noise components are within 2.5. Thresholding on j^{th} wavelet coefficient of level i, c_j^i will obey the rule which can be given as

$$c_j^i = \begin{cases} 0, |c_j^i| < T_i \\ sign[c_j^i][|c_j^i| - T_i], |c_j^i| > T_i \end{cases} \tag{1.2}$$

where

sign$[c_j^i]$ denotes sign of c_j^i .

As shown in Eq. 2.5, wavelet transform coefficients of magnitude below threshold for the particular level, are set to zero. Since the magnitude of these detailed coefficients is higher since they carry edge information of the signal, soft thresholding operation will not affect these coefficients. The coefficients which are set to zero usually are the ones which corresponds to noise.

Reconstruct

Finally, the signal is reconstructed using inverse wavelet transform. Compute wavelet reconstruction based on the original approximation coefficients of level 3 and the modified detail coefficients of levels from 1 to 3.

1.3.2 Continuous wavelet transform

The Wavelet transform (WT) is technique of analyzing a signal in both time and frequency domain. A wavelet is a small wave which has its energy concentrated in time to give a tool for the analysis of transient, non-stationary, or time varying phenomenon. Fig. 1.4 is showing

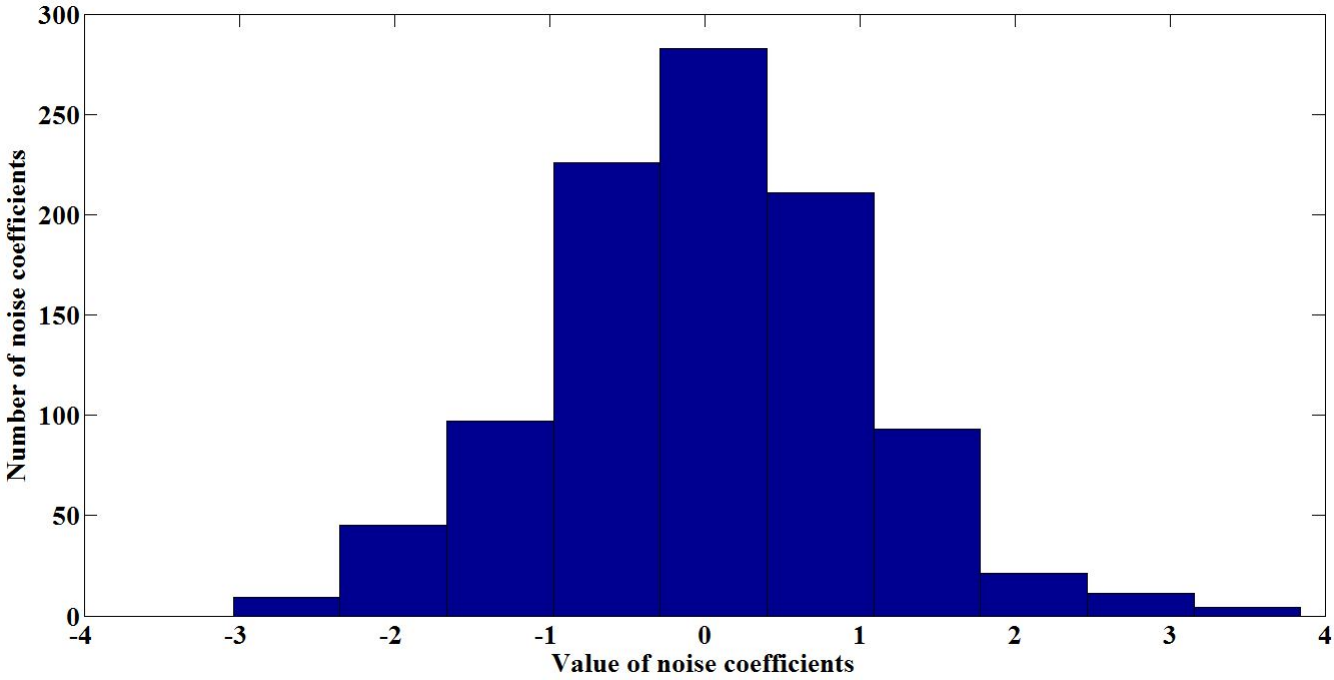

Figure 1.3: Histogram plot showing distribution of noise component

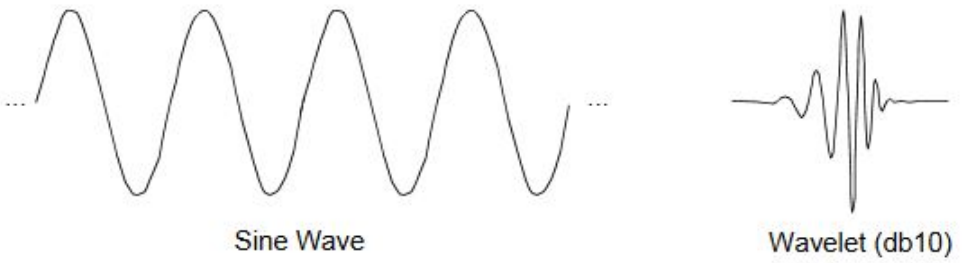

Figure 1.4: A Wave and a Wavelet

the difference between a wave and waveform. Unlike Fourier transform (FT), wavelet transform localize signal in both frequency domain and time domain. The FT assumes that same spectrum occurs for all the time, hence it doesn't localize when a particular frequency characteristics occurred. Shortcoming of FT is removed short time FT (STFT), where fixed window size is taken and FT of a sections of the signals at different time instant are displayed in both frequency and time domain. However, this method has a tradeoff between both frequency and time resolution. When smaller section is considered to get finer time resolution, then frequency resolution get decreased and vice versa. Hence, uniform frequency resolution is undesirable and there is a need of non-uniform frequency resolution which is done in wavelet transform. In WT, different components of the signal are observed in window of different time duration. CWT of $s(t)$ is [9] :

$$CWT(a,\tau) = \frac{1}{\sqrt{a}} \int s(t)\psi^*(\frac{t-\tau}{a})dt, \tag{1.3}$$

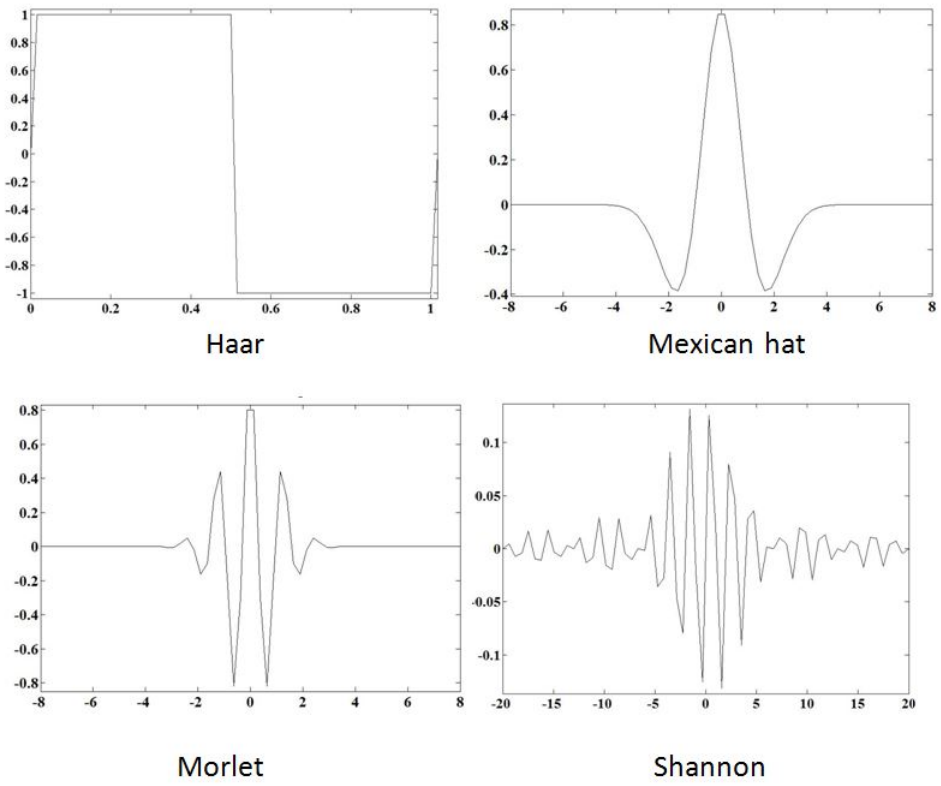

Figure 1.5: Example of Wavelet

where, $\psi^*(t)$ is a mother wavelet, a is the scale factor and τ is the translation. Selection of efficient $\psi^*(t)$ is difficult. In the proposed estimation, Haar wavelet is chosen as mother wavelet because it is highly efficient in localizing and detecting phase transitions in linearly modulated signals. Another reason is that signal amplitude jumps instantaneously at symbol rate and Haar wavelet has similar peculiarity. Haar wavelet is defined as [9] :

$$\psi(t) = \begin{cases} 1, -0.5 < t < 0 \\ -1, 0 < t < 0.5 \\ 0, otherwise \end{cases} \tag{1.4}$$

There are some other wavelets used in wavelet transform are Shannon, Morlet, Mexican hat etc. Fig. 1.5 shows these wavelets. Time-localized event like spikes, transients etc can be captured by WT. WT is also useful in astronomy, acoustics, nuclear engineering, sub-band coding, signal and image processing, neurophysiology, music, magnetic resonance imaging, speech discrimination, optics, fractals, turbulence, earthquake-prediction, radar, human vision, and pure mathematics applications such as solving partial differential equations.

1.3.3 Cyclostationary

Many processes that encountered in nature are not directly periodic in time, although they give rise to some random data whose statistical characteristics vary with time, such processes are called cyclostationary processes. In telecommunications, telemetry, radar, and sonar applications, periodicity is due to modulation, sampling, multiplexing, and coding operations. For example, carrier signal in modulation is periodic in nature but its periodicity is destroyed by modulation process when it is multiplied by modulating signal $x(t)$.

$$z(t) = x(t)cos(2\pi f_0 t). \tag{1.5}$$

where, t is time and f_0 is carrier frequency. If $x(t)$ is wide-sense stationary with auto-correlation function

$$R_x(\tau) = E(x(t+\tau)x(t)), \tag{1.6}$$

where τ is lag. Then the auto-correlation function has periodicity as it is periodic with period $\frac{1}{2f_0}$.

$$E(z(t+\tau)z(t)) = R_x(\tau)\frac{1}{2}[cos(2\pi f_0\tau) + cos(2\pi f_0 t + 2\pi f_0\tau)] \tag{1.7}$$

The stochastic process $x(t)$ is said to be second-order cyclostationary in the wide sense or periodically correlated if its mean

$$m_x(t) \triangleq E[x(t)] \tag{1.8}$$

and auto-correlation function

$$R_x(t,\tau) \triangleq E[x(t+\tau)x(t)] \tag{1.9}$$

are periodic with some period, say $T_0 : m_x(t+T_0) = m_x(t)$ and $R_x(t+T_0,\tau) = R_x(t,\tau)$.

Since, auto-correlation function is periodic in nature it can be represented by Fourier series.

$$R_x(t,\tau) = \sum_{\alpha\in A} R_x(\alpha,\tau)e^{2\pi\alpha t}. \tag{1.10}$$

where the Fourier coefficient $R_x(\alpha,\tau)$ is called cyclic auto-correlation. And α is the cyclic-frequency which meets the condition $A = \alpha : R_x(\alpha,\tau) \neq 0$.

1.4 Outline

The remaining thesis is organized as below:

Chapter 2 deals with the proposed algorithm 1, in which a new method for accurately estimating the symbol rate of any received signal has been proposed. Experiment is tested in both AWGN and Rayleigh fading channel.

Chapter 3 deals with the proposed algorithm 2, in which a new method for accurately identify

the modulation type of any received signal has been proposed. The experiment is tested for BPSK, QPSK, 8-PSK, 4-PAM, and 16-QAM in AWGN while in Rayleigh Fading channel, the experiment is tested for BPSK, QPSK, 8-PSK, and 16-QAM.

Chapter 4 deals with the proposed algorithm 3, a new method for accurately estimating the carrier frequency of any received signal has been proposed.

Chapter 5 deals with detailed complexity analysis based on total number of gate counts.

Chapter 2

Symbol Rate Estimation

2.1 Introduction

In various applications such as surveillance, reconnaissance, position fixing and many other intelligence gathering activities, there is a need of blind estimation of various signal parameters of any received signal. For instance, in wireless communications systems, such signal parameters are carrier frequency, modulation type, symbol rate etc [3–8, 11–15]. In existing systems, these parameters are fixed and are either known at the receiver a priori or estimated using pilot training symbols. In multi-standard environment [16] envisioned for 5G, both these approaches may not be feasible due to the wide range of modulation types and need of training symbols which incurs additional bandwidth and are also prone to eavesdropping attacks. Furthermore, the above approaches are not preferred for military applications. As a consequence, there is a growing interest from the academia as well as industry to design wireless receiver capable of blind estimation of received signal parameters without any prior information and/ or training symbols.

Various algorithms have been proposed for symbol rate estimation using wavelet transform, cyclostationarity, filter bank, cyclic correlation, and inverse fourier transform [3–8] [9] [10]. In [3], transient produced from phase changes in the modulated signal are detected using Wavelet transform and then, symbol rate is calculated based on separation between these transients. Though simple and less complex, it requires large bandwidth and high sampling rate for accurate estimation of symbol rate. The method in [3] is further improved in [5] where outputs from different scales of wavelet transform are combined which lead to accurate symbol estimation especially at moderate carrier-to-noise ratio ($>$ 7dB) and does not require a large oversampling rate. Noise mitigation of the symbol rate estimator is improved in [6], using continuous wavelet transform (CWT) of baseband signal instead of passband signal. A method is proposed in [7] for the parameter estimation of intercepted phase-shift keying (PSK) signals based on cyclic auto-correlation at low SNR. However, the computational complexity of this algorithm is large. Good performance of symbol rate estimation is achieved in [10], by low pass filtering the received signal followed by processing it using a fourth order nonlinear block. Symbol rate is estimated

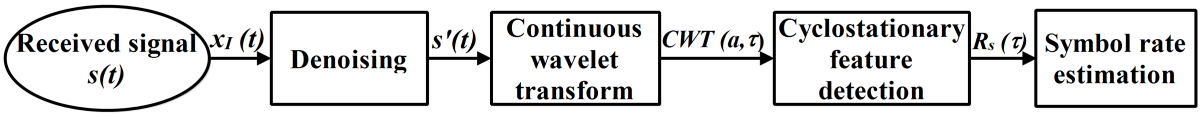

Figure 2.1: Flow diagram of proposed symbol rate estimator

from the spectral peak of nonlinear outputs. However owing to high computational complexity the practical implementation of this algorithm is very arduous task. Furthermore, although most of the estimators perform well at moderate to high SNR but the performance degrades significantly at low SNRs.

In this paper, we alleviate the above drawbacks by proposing a new method to blindly estimate the symbol rate of a received signal. The proposed algorithm exploits excellent localization property of wavelet transform along with superiority of cyclostationary feature detection in low SNR environment. Simulation and gate count complexity results validate the superiority of the proposed algorithm over other algorithms proposed in literature.

The remainder of this paper is organized as follows. Section II is devoted to developing the proposed symbol-rate estimation algorithm. Section III reports the simulation results and compares the performance of the proposed algorithm with that of the continuous wavelet transform (CWT) based algorithm [3–6] and cyclostationary feature detection (CFD) based algorithm [7] based approaches for different modulation types (16-PSK and 16-QAM). In section IV, gate count complexity analysis is presented. Conclusion and future works are drawn in section V.

2.2 Symbol Rate Estimator

In this section, the proposed symbol rate estimator is discussed. The symbol rate estimation can be categorized into three stages , i.e. 1) Denoising 2) CWT and 3) Cyclostationary feature detection (CFD), as shown in Fig. 2.1. Digital bandpass modulation techniques such as Quadrature amplitude modulation (QAM) and phase shift keying (PSK) have two components, in-phase component (I) and quadrature component (Q). The proposed method exploits cyclostationary behavior of I-component of the received signal to estimate its symbol rate. Thus, Q-component of the received signal is not required in the proposed estimation. In the first stage, I component of the down-converted received signal is denoised to improve the SNR of the signal. Denoised signal is then transformed into wavelet domain by applying CWT. Finally, detecting the cyclostationary features of the signal in Wavelet domain, the symbol rate is estimated.

In the following subsections , the proposed symbol rate estimator is discussed in detail. In Section 2.2.1, the signal model is discussed followed by denoising of received signal in section 2.2.2. CWT of the denoised signal is discussed in Section 2.2.3. Finally, estimation of symbol rate using cyclostationary feature detection is presented in section 2.2.4.

2.2.1 Signal Model

The down-converted base-band signal at the receiver can be written as

$$x(t) = s(t) + n(t), \tag{2.1}$$

where $s(t)$ is the transmitted signal and $n(t)$ is independent of signal component, represents additive white gaussian noise (AWGN) with mean zero and variance σ_n^2. $s(t)$ can be written as[1]

$$s(t) = A(t)e^{j\emptyset(t)}, \tag{2.2}$$

where

$$\emptyset(t) = \sum_{i=1}^{M} \alpha_i \Pi(t - iT_s), \tag{2.3}$$

$$\alpha_i \in \{n\frac{\pi}{8}\},$$

$$n \in [0, 15]\,.$$

$A(t)$ and $\emptyset(t)$ represent amplitude and phase of the received signal at time t. For ease of analysis, we assume that $s(t)$ is a 16-PSK modulated signal hence $A(t) = A$. M represents the number of symbols, T_s is the symbol period, $\Pi(t)$ is the unit pulse function of duration T_s.

2.2.2 Wavelet Denoising of Received Signal

Denoising is a method of reducing the noise from received signal which has been contaminated due to AWGN. Conventionally, fast Fourier transform has been preferred for denoising operation [8]. However, it leads to loss of high frequency component in the received signal. Hence, in the proposed method, denoising is accomplished by applying discrete wavelet transform on I component of received signal $x_I(t)$. To remove AWGN from the received signal, five level discrete wavelet transform (DWT) is considered and 'haar' is taken as mother wavelet [17]. Using this, we obtain an approximation coefficients (having low frequency components) and 5 level detailed coefficients (having high frequency components). Then, soft thresholding is applied on all the detailed coefficients where the threshold (T_i) for i^{th} level is related to variance, σ_i^2 and is given by,

$$T_i = \gamma_i \sigma_i, \tag{2.4}$$

where

γ_i is a level factor.

[1] In this paper, the analytical results have been obtained by assuming that 16-PSK modulated signal was transmitted by transmitter. This results can be easily extended to any other linearly modulated signal.

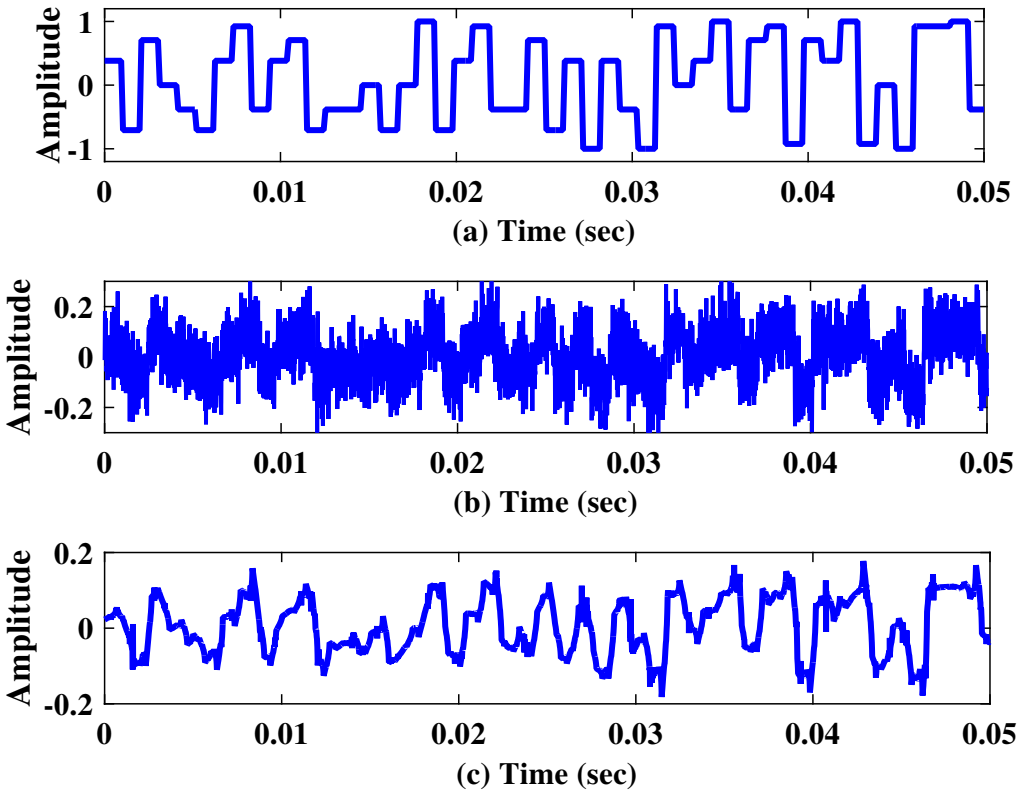

Figure 2.2: (a).I component of the transmitted 16-PSK signal with symbol rate of 955.5 Hz (b).I Component of the received 16-PSK signal at SNR= 2dB (c).De-noised version of the received signal

Thresholding on j^{th} wavelet coefficient of level i, c_j^i will obey the rule which can be given as

$$c_j^i = \begin{cases} 0, |c_j^i| < T_i \\ sign[c_j^i][|c_j^i| - T_i], |c_j^i| > T_i \end{cases} \tag{2.5}$$

where

$$\text{sign}[c_j^i] \text{ denotes sign of } c_j^i \ .$$

As shown in Eq. 2.5, wavelet transform coefficients of magnitude below threshold for the particular level, are set to zero. Since the magnitude of these detailed coefficients is higher since they carry edge information of the signal, soft thresholding operation will not affect these coefficients. The coefficients which are set to zero usually are the ones which corresponds to noise. Finally, the signal is reconstructed ($s^{'}(t)$) using inverse wavelet transform. Fig. 2.2 shows the effect of denoising on received signal [17]. By comparing Fig. 2.2(b) and Fig. 2.2(c), we can say that effect of noise is reduced and original signal (shown in Fig. 2.2(a)) is reconstructed (shown in Fig. 2.2(c))

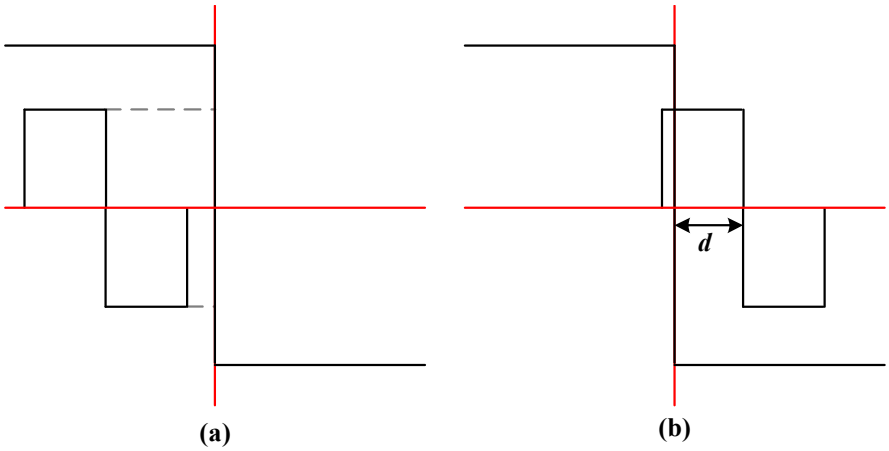

Figure 2.3: Haar wavelet positioning in a PSK signal

2.2.3 Wavelet Transform

For ease of analysis, all the derivations hereafter are done using $s(t)$ instead of I-component of $s(t)$. CWT of $s(t)$ is [9] :

$$CWT(a,\tau) = \frac{1}{\sqrt{a}} \int s(t)\psi^*(\frac{t-\tau}{a})dt, \tag{2.6}$$

where, $\psi^*(t)$ is a mother wavelet, a is the scale factor and τ is the translation. Selection of efficient $\psi^*(t)$ is difficult. In the proposed estimation, Haar wavelet is chosen as mother wavelet because it is highly efficient in localizing and detecting phase transitions in linearly modulated signals. Another reason is that signal amplitude jumps instantaneously at symbol rate and Haar wavelet has similar peculiarity. Haar wavelet is defined as [9] :

$$\psi(t) = \begin{cases} 1, -0.5 < t < 0 \\ -1, 0 < t < 0.5 \\ 0, otherwise \end{cases} \tag{2.7}$$

Selection of optimal scale is difficult, as it requires a large bandwidth and oversampling rate to produce good estimate. As suggested in [3], to reduce the complexity of algorithm and to improve the performance of estimator, coefficients at several scales are combined before estimation. From Fig. 2.3(a), it is quite obvious that when haar wavelet is within the symbol then Haar Wavelet Transform (HWT) of 16-PSK signal with initial phase ϕ can be calculated as,

$$CWT(a,\tau) = \frac{1}{\sqrt{a}}[\int_{\frac{-a}{2}}^{0} Ae^{j\phi(t)}dt - \int_{0}^{\frac{a}{2}} Ae^{j\phi(t)}dt] \tag{2.8}$$

$$= 0.$$

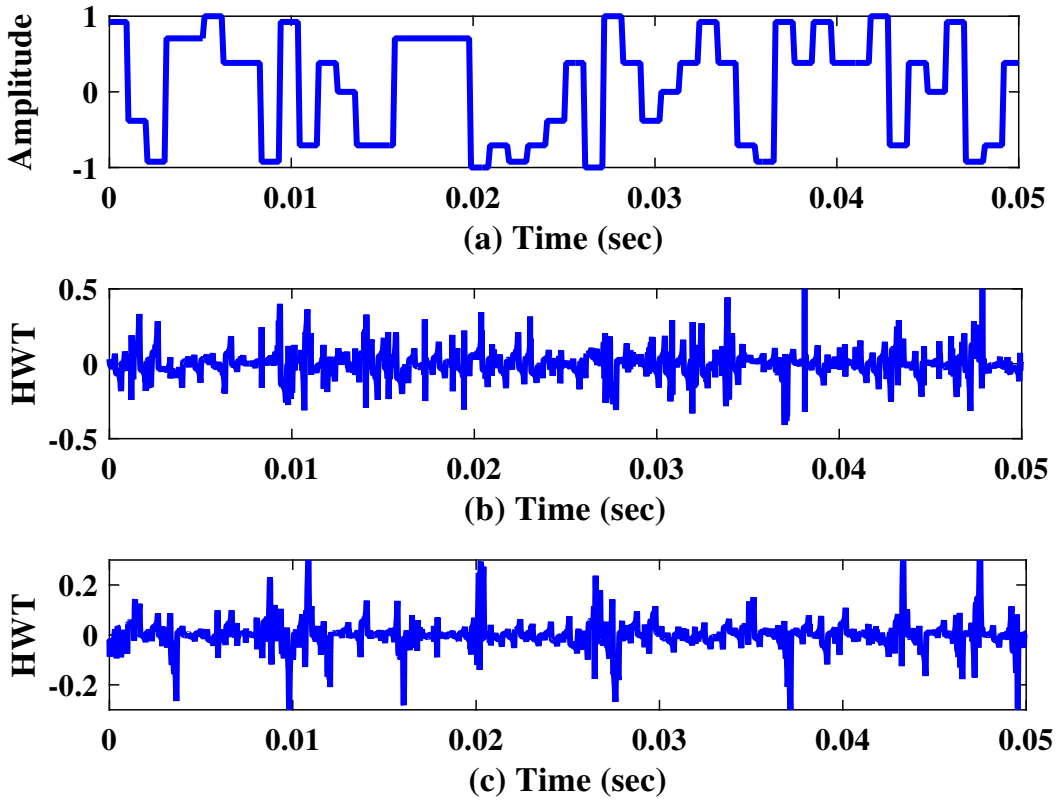

Figure 2.4: (a).I-component of the received 16-PSK signal, (b).Plot of CWT of the received denoised signal at SNR= 2dB, (c). Plot of CWT of the received denoised signal at SNR= 15dB

If there is phase change of π (from Fig. 2.3(b)) then,

$$CWT(a,\tau) = \frac{1}{\sqrt{a}}[\int_{\frac{-a}{2}}^{d} Ae^{j\phi(t)}dt + \int_{d}^{0} Ae^{j(\phi(t)+\alpha)}dt \tag{2.9}$$

$$- \int_{0}^{\frac{a}{2}} Ae^{j(\phi(t)+\alpha)}dt]$$

$$= \frac{A}{\sqrt{a}}[2d + a].$$

From (8) and (9), it is quite obvious that the HWT coefficients change with phase change of 16-PSK signal. Hence, HWT can be used to detect phase transition of 16-PSK signal. Further, it is obvious that HWT can localize the phase change. From Fig. 2.4, it can be observed that each phase transition in the received signal leads to spike. By measuring the smallest time difference between adjacent spikes, symbol rate can be estimated. However, Fig. 2.4(b) also shows that at low SNR (2dB) there are several unwanted spikes. Such spikes leads to inaccurate estimation of symbol rate at low SNR. Hence it is difficult to estimate symbol rate at low SNR.

2.2.4 Symbol Rate Estimation Using Cyclic Autocorrelation

Since HWT does not transform the phase of 16-PSK signal, it is still a cyclostationary random process. Hence, Cyclostationary behavior of HWT of 16-PSK will be same as $s(t)$. Thus its autocorrelation function is,

$$R_s(\tau) = E[s(t)s(t+\tau)] \tag{2.10}$$
$$= A^2 E[e^{j\emptyset(t)} e^{j(\emptyset(t+\tau))}],$$

where τ is delay. Cyclic autocorrelation of $s(t)$ is

$$R_s^\alpha(\tau) = A^2 R_\emptyset^\alpha(\tau), \tag{2.11}$$

where α is cyclic frequency and $R_\emptyset^\alpha(\tau)$ is Cyclic autocorrelation of $\emptyset(t)$. From cyclostationarity of 16-PSK signal [7],

$$\alpha = \frac{k}{T_s}, \tag{2.12}$$

where k is integer, T_s is symbol rate.

From Fig. 2.5, it can be observed that there are peaks at every $\alpha = \frac{k}{T_s}$. Hence symbol rate can be extracted from above. From Fig. 2.5, it can be observed that as SNR decreases, level of peaks are going down. Hence, at low SNR it is very difficult to estimate symbol rate due to low level of peaks. As a result performance will get better with SNR.

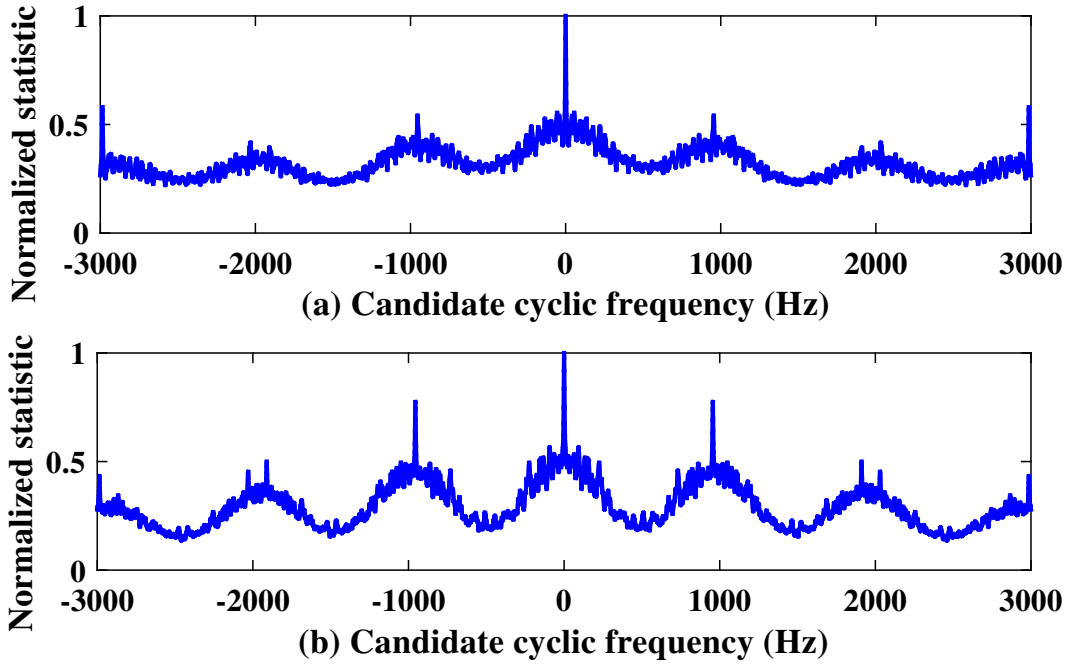

Figure 2.5: Illustration of symbol rate estimation using the proposed algorithm for transmitted symbol rate of 955.5 Hz at (a). SNR= 0dB, and (b).SNR= 15dB.

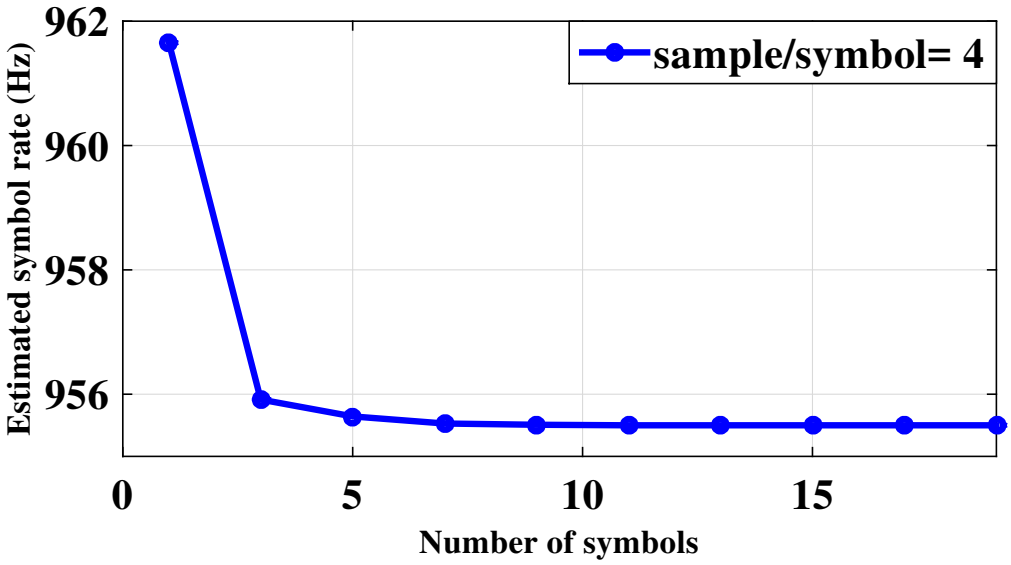

Figure 2.6: Symbol rate estimation for different number of transmitted symbols at SNR=6dB.

2.3 Simulation Results

In order to evaluate the performance of the proposed algorithm, a linearly modulated signal is assumed to be transmitted. It is also assumed that the carrier frequency estimation is ideal or the receiver has *priori* knowledge of the carrier frequency. To check the performance of estimator, signal with symbol rate = 955.5Hz is transmitted. For validation, the proposed algorithm is compared with other algorithms such as CWT based algorithm, and CFD based algorithm. Further, the performance of proposed algorithm is also evaluated when denoising feature is not incorporated. The performance is measured based on percentage error and success rate over 10000 iterations. Percentage error is defined as $|f_s - f_s^{'}| \times 100/f_s$, where f_s and $f_s^{'}$ are symbol rate and estimated symbol rate respectively. Received signal is assumed to be contaminated due to AWGN channel.

Fig. 2.6 plots variation of symbol rate estimation with number of received symbols. Number of samples per symbol are taken to be 4. From Fig. 6 it is quite obvious that 30 received samples (i.e 7 symbols) are sufficient for correct estimation of the symbol rate at 6dB SNR. Fig. 7 shows the symbol rate error performance of CFD based algorithm [7], CWT based algorithm [6], proposed algorithm with and without denoising in terms of percentage error for wide range of SNR. The transmitted signal is assume to be modulated using BPSK. It can be observed from Fig. 2.7 that the proposed algorithm outperforms all other algorithms except at high SNRs ($>$ 6dB) where CFD based algorithm is slightly better. It can also be observed that denoising leads to significant improvement in estimation performance at low SNRs. Furthermore, the percentage error in the proposed algorithm remains same for SNR $>$ -1 dB. This is due to the fact that proposed algorithm leads to prominent peaks in the signal obtained from cyclostationary stage which aids in accurate symbol rate estimation. Such peak estimation is difficult when SNR $<$-1 dB which can also be deduced from poor performance of CFD based algorithm.

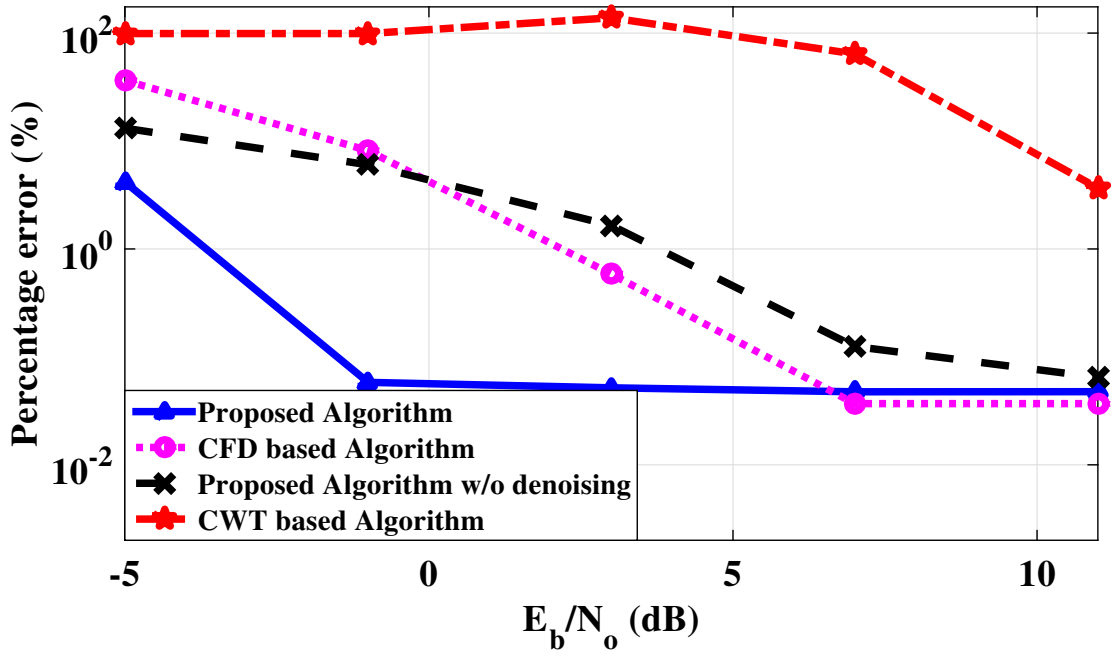

Figure 2.7: Comparison of symbol rate estimation accuracy of different estimators based on probability error for transmitted signal with BPSK modulation, symbol rate of 955.5 Hz and pulse shaping filter with roll-off factor of 0.3.

Fig. 2.8 shows the performance comparison in terms of success rate of proposed algorithm with filter bank based algorithm [10] and cyclic correlation based algorithm [11] for wide range of SNR. It can be observed that the proposed algorithm performs better than others at low SNRs. At high SNRs, performance of all these algorithms are almost same. Note that implementation complexity of filter bank based algorithm is high which makes the proposed algorithm a better alternative over filter bank based algorithm.

Performance comparison of the proposed algorithm for different modulation schemes is shown in Fig. 2.9. It is obvious from the plot that performance of algorithm improves with increase in order of modulation. It is because for a fixed window size, the number of symbol transition will be different for different modulation schemes. Further, it will increase with increase in modulation order. Since, the number of glitches after CWT stage are basically due to symbol transition, hence it will also increase with modulation order. As a result, quantity of information before CFD stage is more for 64-QAM, which results into better performance of 64-QAM than other lower order modulations. In case, if there are almost same number of symbol transition for each modulations (Appendix A), the performance of higher modulation will be worse than those of lower modulation as expected. Since, in this case higher order modulation scheme posses less number of spikes when compared to lower order modulation scheme, as less number of symbol transitions possessed by higher order modulation schemes.

Fig. 2.10 shows the performance comparison of 16-PSK and 16-QAM. It is clear from the figure that at low SNRs the performance of the proposed algorithm is almost same for both modulation schemes. At higher SNRs, 16-PSK is performing slightly better than 16-QAM. However, 16-

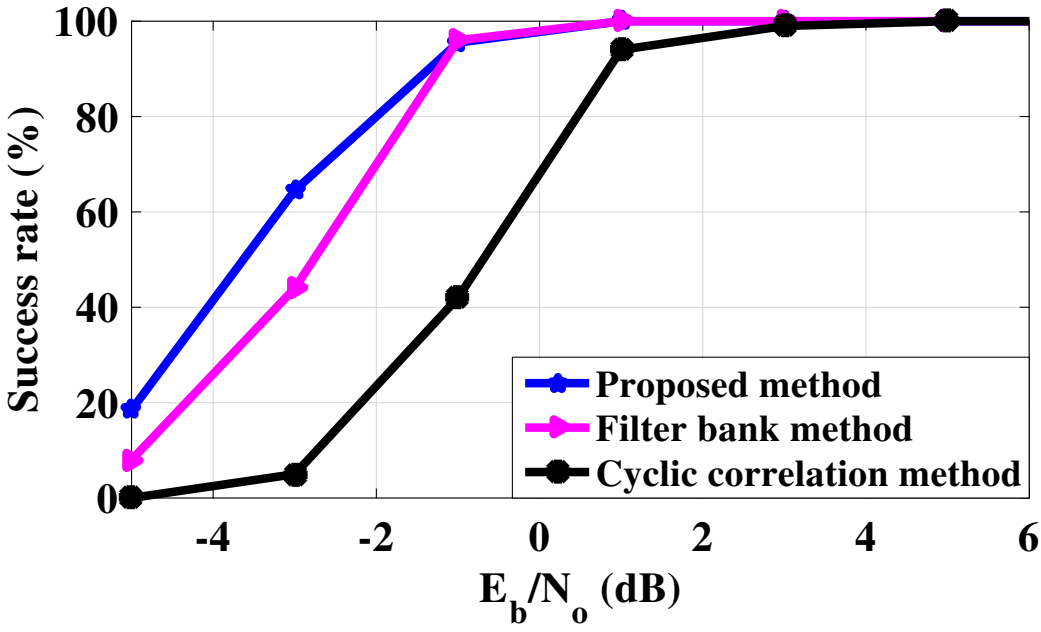

Figure 2.8: Comparison of symbol rate estimation accuracy of different estimators based on success rate for transmitted signal with BPSK modulation, symbol rate of 955.5 Hz and pulse shaping filter with roll-off factor of 0.3.

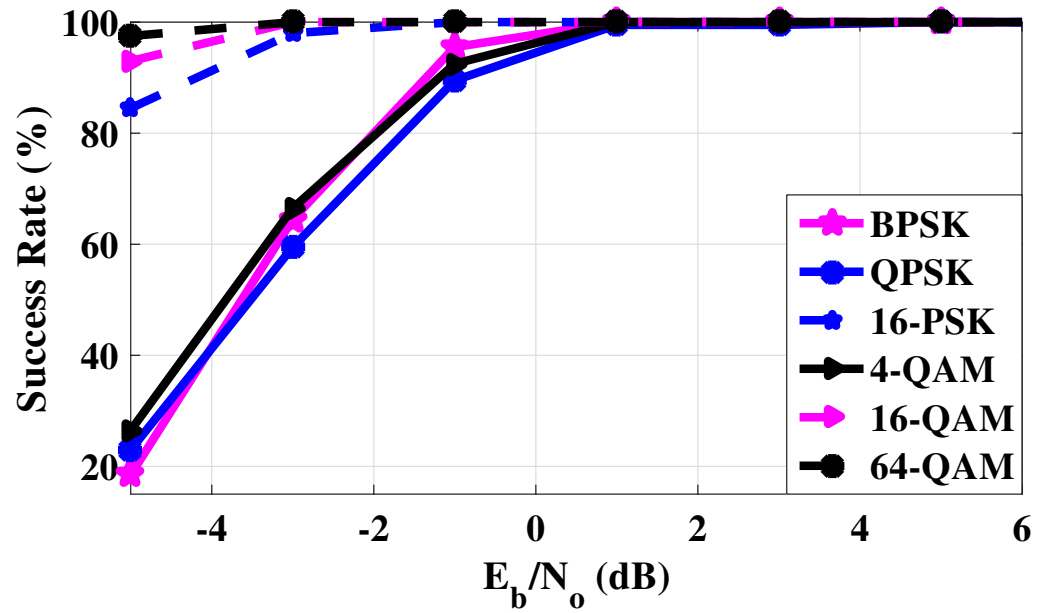

Figure 2.9: Comparison of symbol rate estimation accuracy of proposed algorithm for transmitted signal with different modulation schemes with symbol rate of 955.5 Hz and pulse shaping filter with roll-off factor of 0.3.

QAM is outperforming 16-PSK when denoising is not taken into account. This is due to the fact that the denoising is more effective when the signal is 16-PSK modulated. Apart from above, it is also obvious that the proposed algorithm outperforms conventional CFD based algorithm at low SNRs. At approximately 0dB the difference is around 20%. This difference decreases at higher SNRs. This shows that the proposed algorithm is quite effective at low SNRs. Another point to

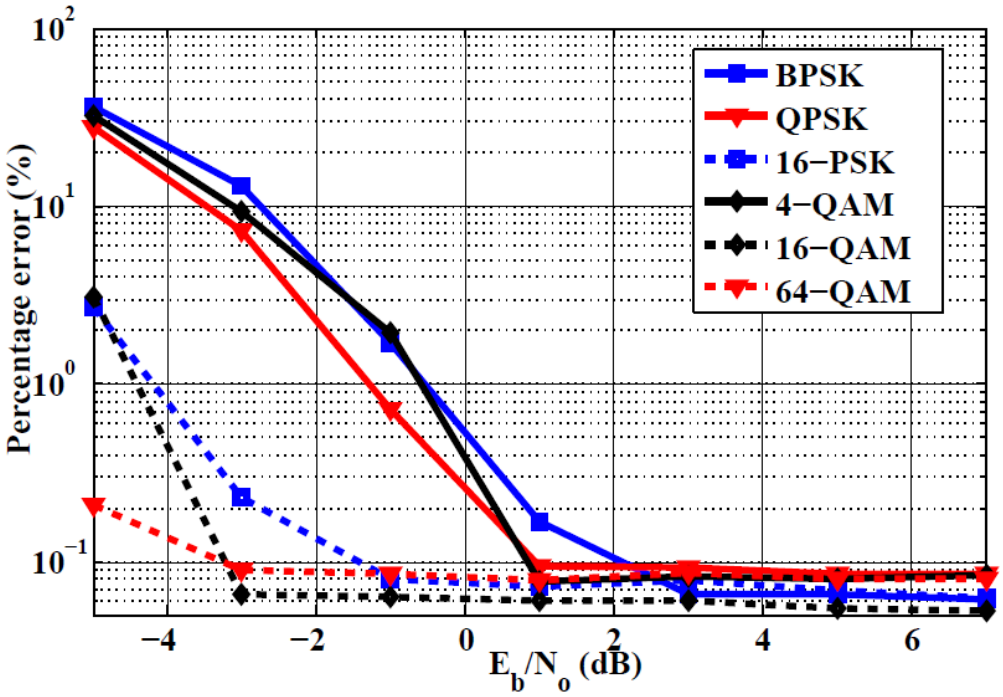

Figure 2.10: Comparison of symbol rate estimation accuracy of proposed algorithm for transmitted signal with different modulation schemes with symbol rate of 955.5 Hz and pulse shaping filter with roll-off factor of 0.3.

note is that, the proposed algorithm achieve significant performance improvement for 16-QAM modulation even at 8dB SNR (when compared with conventional CFD based algorithm). Hence for 16-QAM modulated signal this algorithm is effective even for moderate SNR levels.

Fig. 2.11 shows the performance of estimator for different number of transmitted symbols. It can be observed that performance varies with SNR. At low SNRs ($<$ 3dB), the estimation performance improves with increase in number of symbols. Further, there is gap of almost 2dB in the performance. Signal with 100 symbols has a percentage error of 0.1% at 3dB SNR whereas signal with 200 symbols has the same error at 1dB SNR. However, after saturation point ($\approx$ 4dB) there is no significant difference between the performance with different N (N=100, 200, and 600). This is due to the fact that at high SNRs significant peaks are observed after CFD stage and accurate symbol rate can be estimated for a signal with fewer number of symbols.

Fig. 2.12 shows the effect of symbol rate estimator in multi-path Rayleigh fading channel. The performance of estimator is tested for BPSK, QPSK, 16-PSK, 16-QAM, and 64-QAM modulation schemes. For QPSK, the percentage error is 0.1% at 17dB SNR, however other modulation schemes except 16-QAM possess same error at around 22dB-23dB SNR. At 23dB SNR, except 16-QAM, all other modulation scheme have same estimation performance i.e around 0.1 percentage error at $\approx$ 23dB SNR. From 23dB onwards, there is no significant difference in the estimation performance of the different modulation schemes. Performance of 16-QAM is worse as compared to other modulation schemes. When compared with BPSK, the difference in percentage error may go upto 9.9% which then nullifies at 29dB SNR. At around 29dB, all

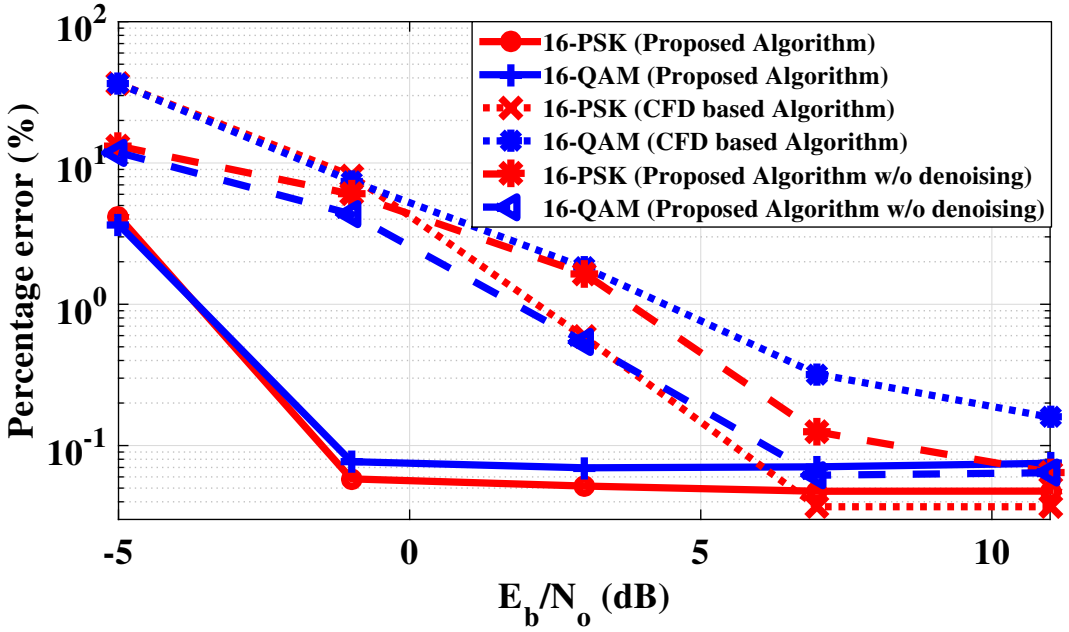

Figure 2.11: Comparison of symbol rate estimation accuracy of different estimators for transmitted signal with 16-PSK modulation and 16-QAM modulation with symbol rate of 955.5 Hz and pulse shaping filter with roll-off factor of 0.3.

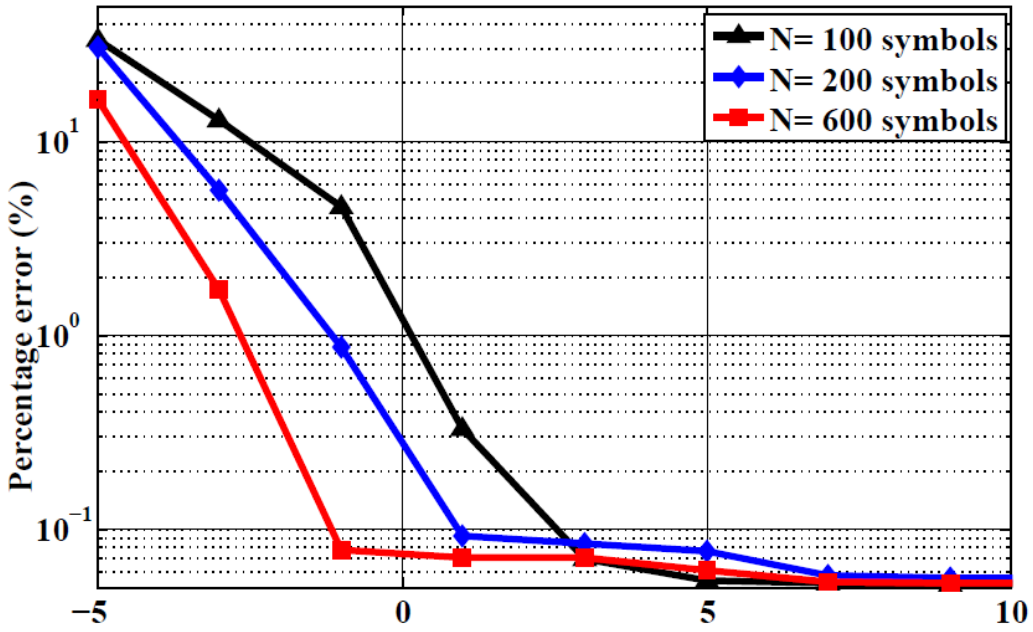

Figure 2.12: Comparison of symbol rate estimation accuracy of proposed estimator for transmitted signal in AWGN with BPSK modulation with symbol rate of 955.5 Hz and pulse shaping filter with roll-off factor of 0.3

the modulation schemes are performing almost same and has an estimation of approximately 0.05%. Thus symbol rate estimation of higher order modulation schemes are affected more in the multi-path fading channel.

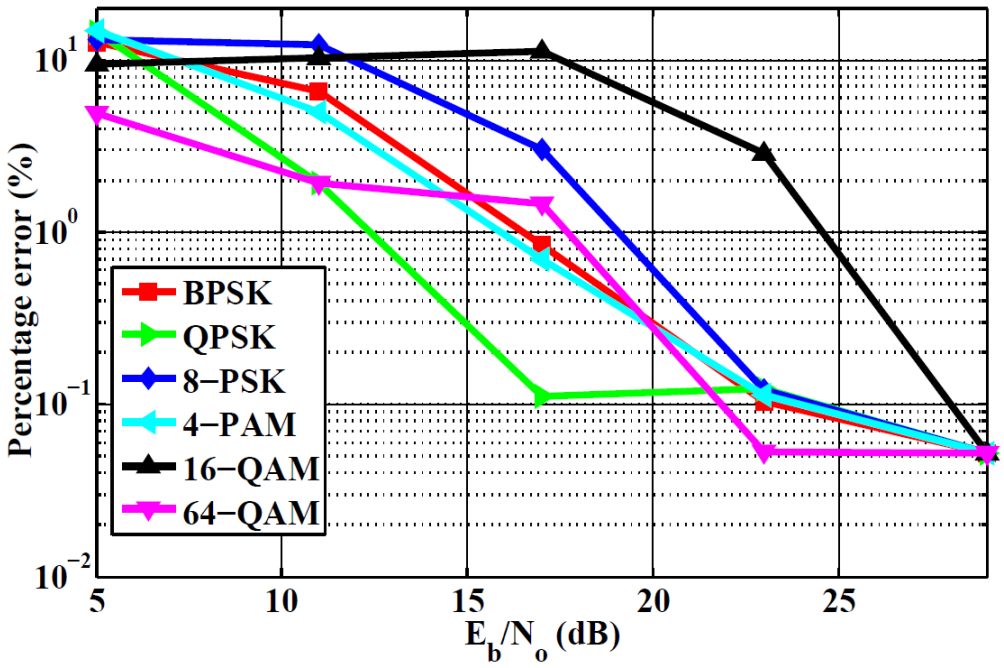

Figure 2.13: Comparison of symbol rate estimation accuracy of different estimators for transmitted signal in Rayleigh fading channel with symbol rate of 955.5 Hz and pulse shaping filter with roll-off factor of 0.3

Fig. 2.13 compares the estimation performance of the proposed scheme for 16-PSK and 16-QAM modulation in AWGN and Fading channel. It can be observed that at 5dB SNR, there is difference of approximately 8% between the estimation in AWGN and fading channel for 16-PSK modulation whereas there is difference is 9.37% for 16-QAM modulation.

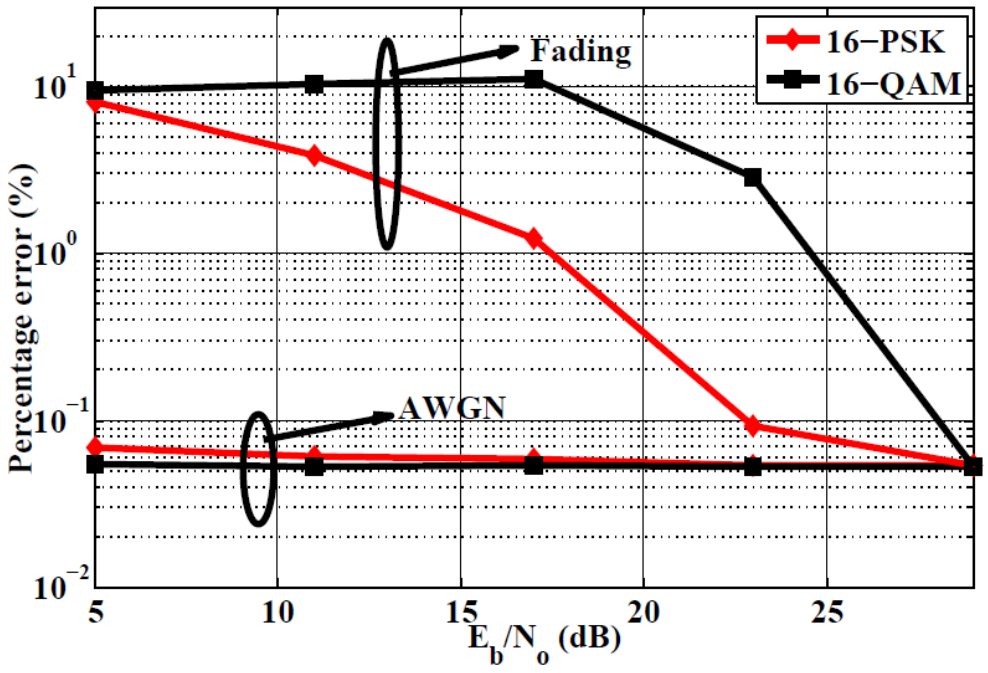

Figure 2.14: Comparison of symbol rate estimation accuracy of estimators in AWGN and Rayleigh fading channel for transmitted signal with 16-PSK and 16-QAM modulation with symbol rate of 955.5 Hz and pulse shaping filter with roll-off factor of 0.3

Chapter 3

Modulation Classification

3.1 Introduction

In this chapter, a new automatic modulation classifier (AMC) for PSK, PAM and QAM signals is proposed. These modulation schemes are widely used in modern digital communication. For example, commonly QAM is used in digital microwave communication [18] and telephone line modem [19, 20]. These categories of modulation are also used in technologies for high internet access like ISDN, ADSL, and HDSL [21]. AMC is important for the receiver that has no, or limited, knowledge of signal received as it is intermediate step between signal detection and demodulation. In modern communication AMC is widely used in adaptive modulation [22, 23], where the modulation schemes are switched dynamically with the change in channel. It means modulation type of transmitted signal can change with change in state of channel, like whenever channel is clean higher level modulation can be transmitted, and low level modulation scheme can be transmitted in noisy channel. Information about modulation type of transmitted signal is must for receiver in order to demodulate at receiver side to extract the original transmitted message. One way to do this is by sending a pilot signal along with the original message to inform the receiver about the modulation type [24, 25]. However, the above technique is applicable but it comes at the cost of loss of bandwidth efficiency and reduction in data throughput due to periodically sending pilot signals that carry no data, especially for those having small data blocks. Smart receiver can remove this drawback where some properties of the received signal can be used to identify modulation. That is why AMC is a topic of huge interest for both military and civilian application [26], where there is no prior agreement between transmitter and receiver. Due to unavailability of any prior knowledge of incoming signal in non-cooperative environment, the identification of incoming signal is a difficult task. AMC is also getting popular due to recent development in software defined radio (SDR) as single SDR can handle multiple modulations [27].

In recent years interest in modulation recognition has increased with the emergence of new communication technologies. There are many techniques published in literature for modulation identification. Generally modulation classification technique can be divided into two main

approaches:

- Maximum likelihood (ML)
- Feature-based (FB) method

In first approach all the methods are based on likelihood function which depend on transmitted symbols, signal and channel parameters. In this method, initially all the modulation format are assumed to be equally likely and finally the modulation format is selected which maximizes likelihood function [28–30]. In feature based method, selectors design a specific feature which uniquely represent each modulation format. Decision of selection is based on the value of features used in the design. The implementation of feature based method is easier if it is designed well. In paper [31], maximum-likelihood (ML) based automatic modulation classification is done under both coherent and non-coherent conditions. Under coherent condition all signal parameters (symbol rate, carrier frequency, carrier phase, pulse shape, SNR and timing offset) are known. However, under non-coherent condition all signal parameters are known except carrier phase. Loss of 3dB exhibited in the non-coherent case as compared to coherent case. In paper [32], theoretical performance of ML modulation classifier is obtained. It can work under ideal conditions, which can serve as an upper bound performance of any classifier. Similar theoretical analysis is done in paper [33]. In addition, the study of asymptotic behavior is done which shows that ML classifier is capable to reach zero error rate when number of available data symbols goes to infinity. The method suffers from model mismatch with respect to carrier frequency and phase offsets. ML technique can be further divided into three approaches: Average Likelihood Ratio Test (ALRT [34], Generalized Likelihood Ratio Test (GLRT) [34] and Hybrid Likelihood Ratio Test (HLRT) [34]. Although ML approach lead to optimal solution but feature based approaches are preferred because of its low complexity and satisfactory performance. Likelihood based approach assume prior knowledge about the signals.

In feature based approach, modulations are represented by their representing feature and then these features are used by a machine learning algorithm to detect modulation. Efficiency of the algorithm is decided by the classification power of the algorithm and its simplicity. Some of the feature based technique are as followed:

- Spectrum Analysis-Based Classification Scheme
- Wavelet Transform
- Clustering Algorithms
- Cyclostationary Feature-Based
- High Order Moments (HOMs) and High Order Cumulants (HOCs)

In spectrum analysis-based scheme, modulation can be identified by analyzing spectrum of the unknown signal. In paper [35], a technique of identification of Multiple Frequency Shift Keying

(MFSK) and MPSK using frequency spectrum and phase spectrum is suggested. As Multiple Frequency Shift Keying (MFSK) contains baseband information in different carrier frequency which results into higher magnitude at these frequencies and lower magnitude at other unused frequencies. Likewise, number of phases used in MPSK can be counted from phase spectrum. However, it is difficult to identify all type of modulation from frequency spectrum and phase spectrum. Classification of modulation by taking Fast Fourier Transform (FFT) of received technique is suggested in paper [36], as FFT of BFSK possesses two peaks in the frequency spectrum, 4-FSK shows 4 peak and likewise, M-FSK shows M peaks. And MPSK signals can be classified by calculating ratio of peaks. However, fourier transform works on the assumption that signal is stationary and spectrum is time invariant. For the non-stationary signal, wavelet transform technique is introduced in which signal is analyzed in both frequency domain and time domain, where signal is decomposed into high pass coefficients (detailed coefficients) and low pass coefficients (approximation coefficients) [37, 38]. Modulation class can be identified from detailed coefficients as different modulations contains different details coefficients at same scale. In clustering algorithms, received symbols of unknown signals are grouped into clusters and then modulation type is identified from number of clusters and location of their centroids. Various clustering techniques are suggested in papers [39]. In HOC method value of higher order cumulants are calculated which is different for different modulations. In paper [40], fourth order cumulant is calculated for PSK, PAM and QAM signal under noiseless environment and finally modulation type is identified as different modulation has different HOCs value. Mixed-order moments are used in paper [41] to discriminate between different levels of QAM modulation.

In this chapter we are using symbol rate estimator of chapter 2 to further identify modulation of received signal automatically. The proposed scheme is tested for BPSK, QPSK, 8-PSK, 4-PAM, and 16-QAM modulation types in Additive White Gaussian Noise (AWGN) and flat fading environment. After estimation of symbol rate, modulation identification is done from the histogram of received signal. The proposed method is simple as far as modulation identification part is concerned but overall complexity is high due to the symbol rate estimation part.

The remainder of this paper is organized as follows. Section II is devoted to developing the proposed automatic modulation identification algorithm. Section III reports the simulation results and compares the performance of the proposed algorithm with other algorithms.

3.2 Modulation Classifier

In this section, the proposed modulation classifier algorithm is discussed. The basic stages of this algorithm is same, which are used for symbol rate estimation in chapter 2. The modulation classifier can also be categorized into three stages , i.e. 1) Denoising 2) CWT and 3) Cyclostationary feature detection (CFD), as shown in Fig. 3.1. After estimation of symbol rate, symbols in corrupted received signal are mapped to nearest possible symbol. And finally, modulation type is identified from modified signal.

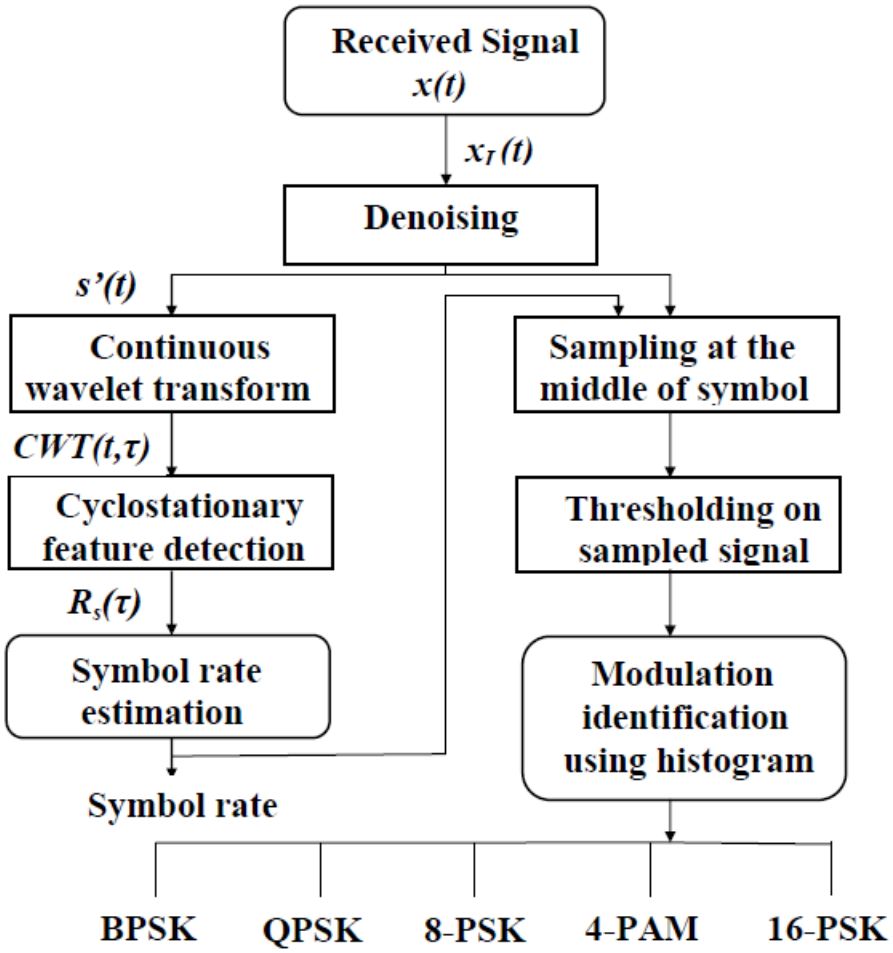

Figure 3.1: Flow diagram of proposed modulation classifier

In the following subsections , the proposed modulation classifier is discussed in detail. Since, all the stages are same which were used in chapter 2, we are not going in details of each stages. In Section 3.2.1, the signal model is discussed followed by denoising of received signal in section 3.2.2. CWT of the denoised signal is discussed in Section 3.2.3. Then estimation of symbol rate using cyclostationary feature detection is presented in section 3.2.4. Finally, identification of modulation type from received signal by using symbol rate is discussed in section 3.2.5.

3.2.1 Signal Model

The down-converted base band signal at the receiver can be written as

$$x(t) = s(t) + n(t), \tag{3.1}$$

where $s(t)$ is the transmitted signal and $n(t)$ is independent of signal component, represents additive white gaussian noise (AWGN) with mean zero and variance σ_n^2. Transmitted signal $s(t)$

can be written as[1] In this chapter, presence of pulse shaping filter at transmitter is not taken into account. However in chapter 3, performance is analyzed by considering the effect of pulse shaping filter.

$$s(t) = A(t)e^{j\emptyset(t)}, \tag{3.2}$$

where

$$\emptyset(t) = \sum_{i=1}^{M} \alpha_i \Pi(t - iT_s), \tag{3.3}$$

$$\alpha_i \in \{n\frac{\pi}{8}\},$$

$$n \in [0, 15]\,.$$

$A(t)$ and $\emptyset(t)$ represent amplitude and phase of the received signal at time t. For ease of analysis, we assume that $s(t)$ is a 16-PSK modulated signal hence $A(t) = A$. M represents the number of symbols, T_s is the symbol period, $\Pi(t)$ is the unit pulse function of duration T_s.

3.2.2 Wavelet Denoising of Received Signal

Denoising is a method of reducing the noise from received signal which has been contaminated due to AWGN. Conventionally, fast Fourier transform has been preferred for denoising operation [8]. However, it leads to loss of high frequency component in the received signal. Hence, in the proposed method, denoising is accomplished using the same technique used in chapter 2. Fig. 3.2 shows the effect of denoising on received signal [17]. By comparing Fig. 3.2(b) and Fig. 3.2(c), we can say that effect of noise is reduced and original signal (shown in Fig. 3.2(a)) is reconstructed (shown in Fig. 3.2(c)). It can be observed from Fig. 3.2, that amplitude of signal is different from those in chapter 2. This happened due to gain of pulse shaping filter used in chapter 2.

3.2.3 Wavelet Transform

CWT of denoised signal will spikes at each phase transitions of received signal. From Fig. 3.3, it can be observed that each phase transition in the received signal leads to spike. From Fig. 3.3(b), it can be observed that at low SNR (2dB)there are several unwanted spikes because of immense noise power.

3.2.4 Symbol Rate Estimation Using Cyclic Autocorrelation

As discussed in chapter 3, since HWT does not transform the phase of 16-PSK signal, it is still a cyclostationary random process. Thus, by exploiting this property cyclic auto-correlation of HWT output is evaluated. As a result, peaks can be observed at every $\alpha = \frac{k}{T_s}$, where α is cyclic

[1] In this paper, the analytical results have been obtained by assuming that 16-PSK modulated signal was transmitted by transmitter. This results can be easily extended to any other linearly modulated signal.

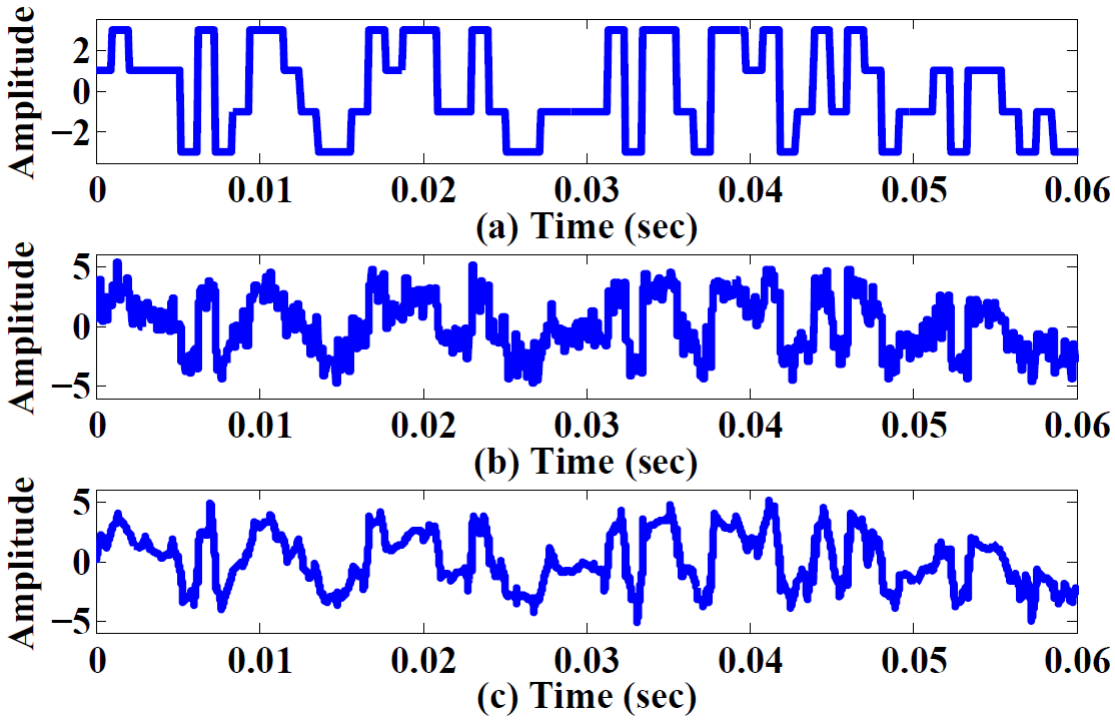

Figure 3.2: (a).I component of the transmitted 16-PSK signal with symbol rate of 955.5 Hz (b).I Component of the received 16-PSK signal at SNR= 2dB (c).De-noised version of the received signal

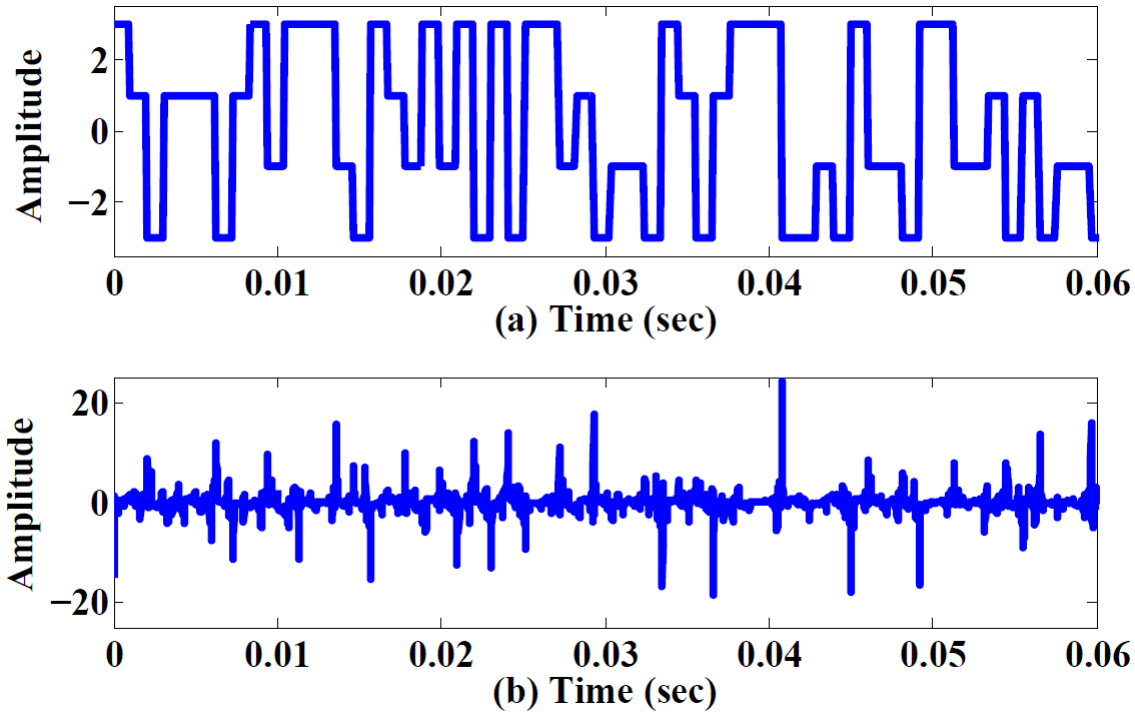

Figure 3.3: (a).I-component of the received 16-PSK signal, (b).Plot of CWT of the received denoised signal at SNR= 2dB

frequency, k is integer and T_s is symbol rate. Peaks are clearly visible from Fig 3.4 which are present at integer multiple of symbol rate. Hence symbol rate can be extracted from above.

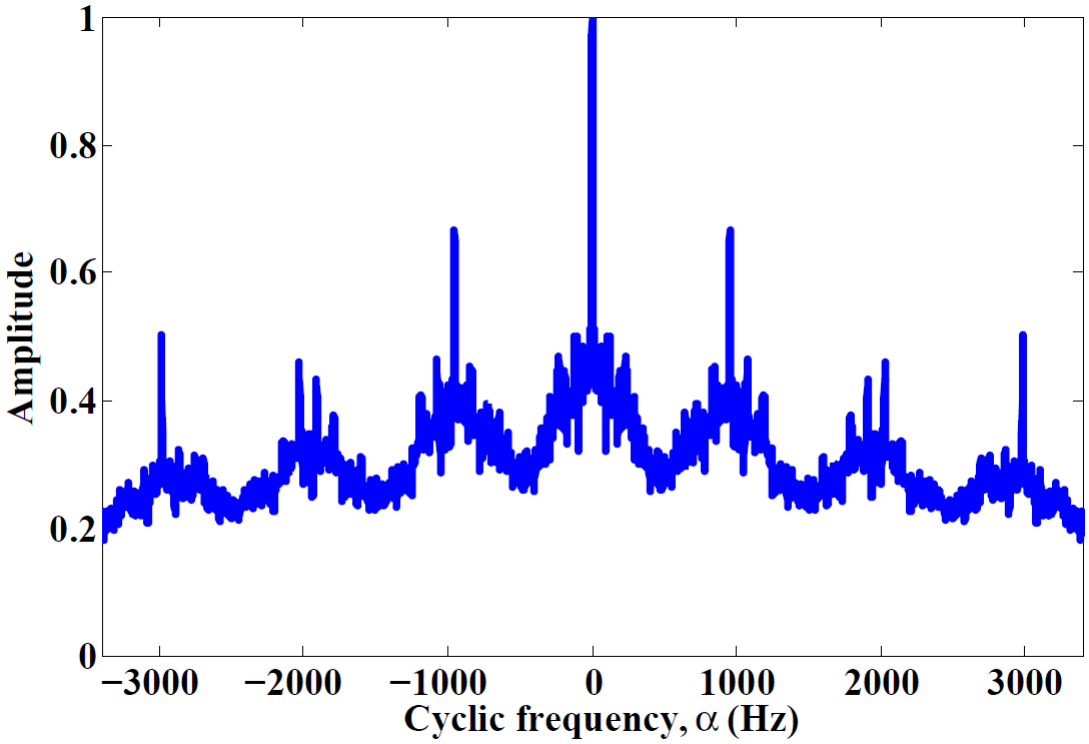

Figure 3.4: Illustration of symbol rate estimation using the proposed algorithm for transmitted symbol rate of 955.5 Hz at SNR= 2dB

3.2.5 Modulation identification using histogram

In this section, we will classify the modulation from histogram plot of received signal after performing some operation on received signal using estimated symbol rate. Since, different modulations give different features (phase, amplitude, etc), so it can be possible to classify modulations from these features. In our proposed technique, we have used I-component of complex envelop of received base-band signal. Block diagram of modulation classification part after symbol rate estimation is shown in Fig. 3.5. Whole classification process is divided into two steps: 1) sampling and digitizing of received signal using estimated symbol rate of chapter 2 and 2) count number of peaks above certain threshold value from histogram plot.

Sampling and digitizing of received signal

Received signal has complex envelop and it is continuous in nature. After estimation of symbol rate($f_s^{'} = \frac{1}{T_S^{'}}$), I component of signal is sampled in the middle of symbol (due to high SNR of signal in the middle of symbol) at the sampling rate equal to symbol rate.

$$x_I(n) = x_I(t) \mid_{nT_s}, \tag{3.4}$$

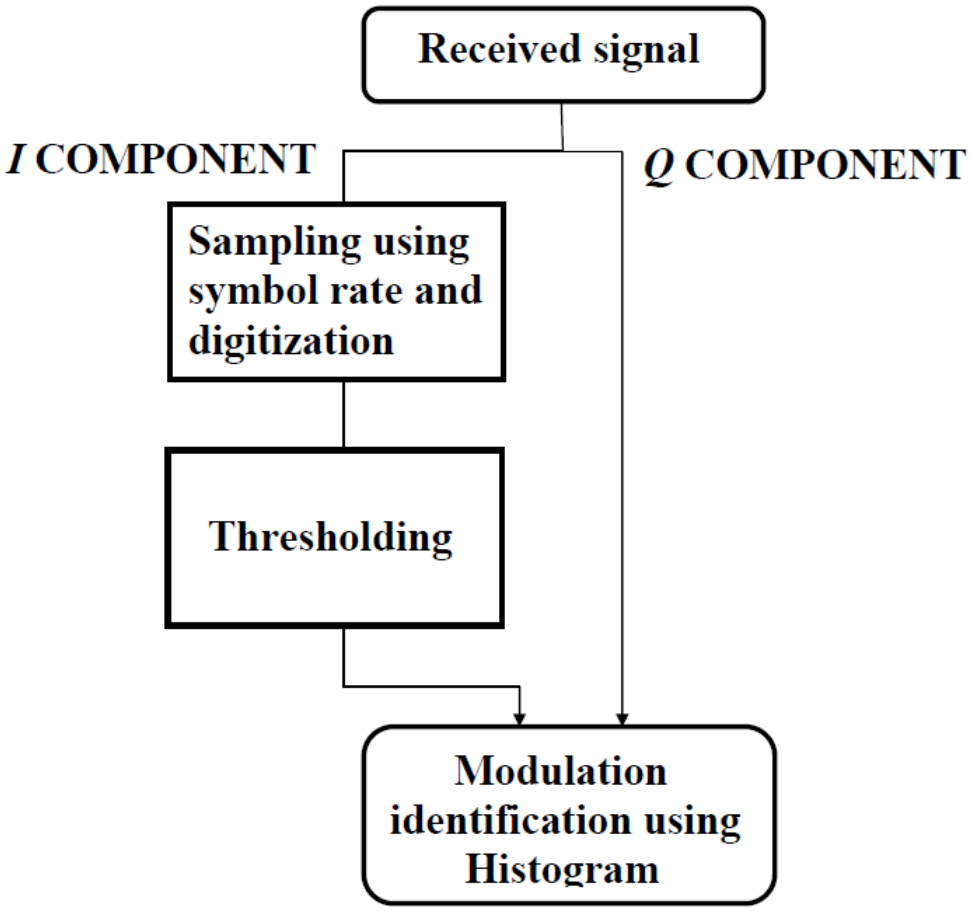

Figure 3.5: Block diagram of modulation classification part after symbol rate estimation

where

$$n = 0, \ldots\ldots N - 1.$$

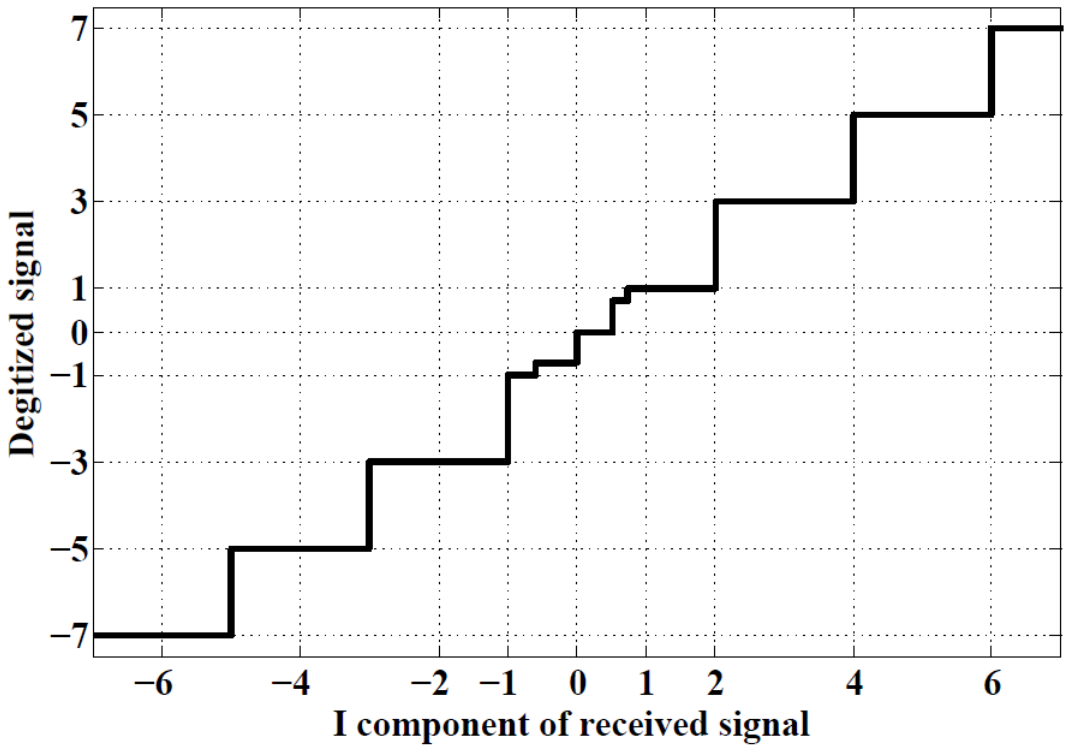

Figure 3.6: Figure showing quantization criteria of received signal

Sampled values are compared with certain values and modified to $s'(n)$ such that (as shown in Fig. 3.7):

$$s'(n) = \begin{cases} 7, 6 < s(n) \\ 5, 4 < s(n) \leq 6 \\ 3, 2 < s(n) \leq 4 \\ 1, 0.73 < s(n) \leq 2 \\ 0.707, 0.5 < s(n) \leq 0.73 \\ 0, -0.5 < s(n) \leq 0.5 \\ -0.707, -0.73 < s(n) \leq -0.5 \\ -1, -2 < s(n) \leq -0.73 \\ -3, -4 < s(n) \leq -2 \\ -5, -6 < s(n) \leq -4 \\ -7, otherwise \end{cases} \tag{3.5}$$

After getting modified sampled values, number of samples per symbol in transmitted signal is estimated, N_s and all the samples within a symbol are made equal to sampled value at middle of the symbol. In this way I component of signal gets quantized as shown in Fig. 3.8.

$$N_s = \frac{\text{sampling rate}}{\text{estimated symbol rate}}, \tag{3.6}$$

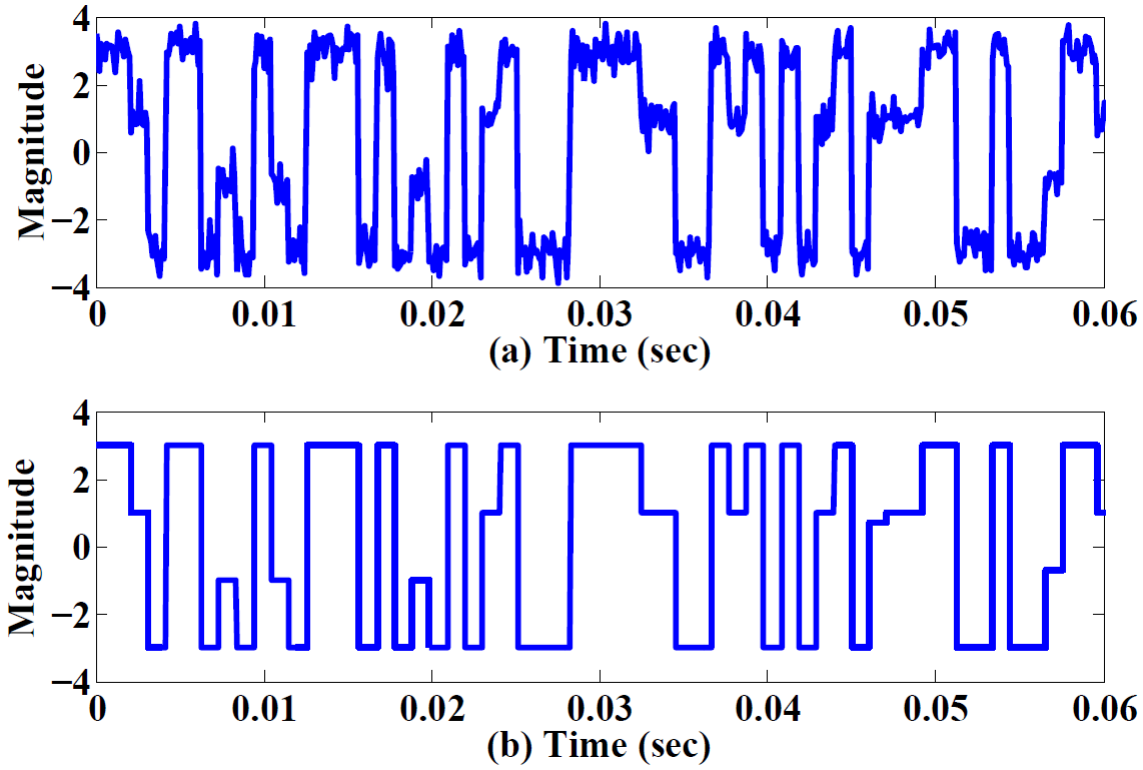

Figure 3.7: I-component of received 16-PSK signal (a).before digitization, (b).after digitization

Thresholding and modulalation detection using histogram

After quantization of signal, we can get ideal constellation diagram of digitized signal which should match the constellation diagram of transmitted signal. However, due to some quantization error we may not get ideal constellation diagram as shown in Fig. 3.8. Hence, there will be some extra symbols which do not match the feature of possible modulation schemes. The challenge is to ignore these extra symbols due to quantization error.

Histogram of quantized signal will give very high values at constellation values which shows that those values are present in large amount. However, there will be some other redundant small values as a result of extra symbols due to quantization error. In histogram plot, x-axis is sample values and y-axis is number of samples corresponding to sample values. To avoid error we need to set a threshold value (γ). Lets say p is number of peaks observed and m_i is number of samples corresponding to i^{th} peak. All peaks corresponding to which number of samples are greater than threshold value can be counted as peaks and other are neglected such that N_p is total number of peaks after satisfying threshold condition.

$$N_p = k, N(m_i > \gamma) = k, \tag{3.7}$$

where

$$i = 1,.....p.$$

$N(m_i > \gamma)$ denotes the number of peaks for which $m_i > \gamma$. As observed from Fig 3.9 number of

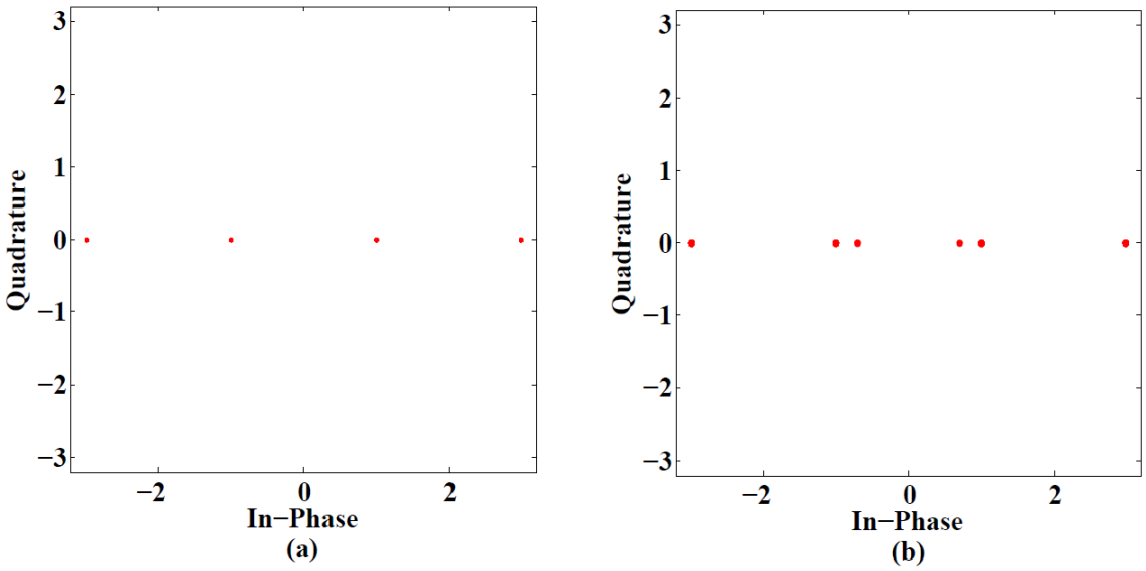

Figure 3.8: Constellation diagram of (a).I-comoponent of transmitted signal, (b).I-comoponent of quantized signal

significant peaks N_p is 2 for BPSK, 3 for QPSK, 4 for 4-PAM and 16-QAM, 5 for 8-PSK. Let β denotes set of sample values at which significant peaks occur then,

$$N_p = \begin{cases} 2, \beta \in \{-1, 1\} \\ 3, \beta \in \{-1, 0, 1\} \\ 4, \beta \in \{-3, -1, 1, 3\} \\ 5, \beta \in \{-1, -0.707, 0, 0.707, 1\} \end{cases} \tag{3.8}$$

Fig. 3.10 compares histogram of signal before digitization and after digitization. Fig 3.11 compares the signal at low SNR and high SNR using histogram. As for 16-PSK there should be four significant peaks (peaks above red line), but due noise at low SNR there are peaks other than 4. Hence at low SNR modulation is not classified correctly. Fig. 3.12 shows the classification tree for modulation. Since,there is no Q-component (s_q) of BPSK and 4-PAM. Hence, they are classified in separate group and rest are defined in other group. After that, they are classified based on number of significant peaks in histogram plot.

3.3 Simulation Results

In order to evaluate the performance of the proposed algorithm, a linearly modulated signal is assumed to be transmitted. It is also assumed that the carrier frequency estimation is ideal or the receiver has *priori* knowledge of the carrier frequency. To check the performance of estimator, signal with symbol rate = 955.5Hz is transmitted with BPSK, QPSK, 8-PSK, 4-PAM, and 16-QAM modulated schemes. For validation, the proposed algorithm is compared with other

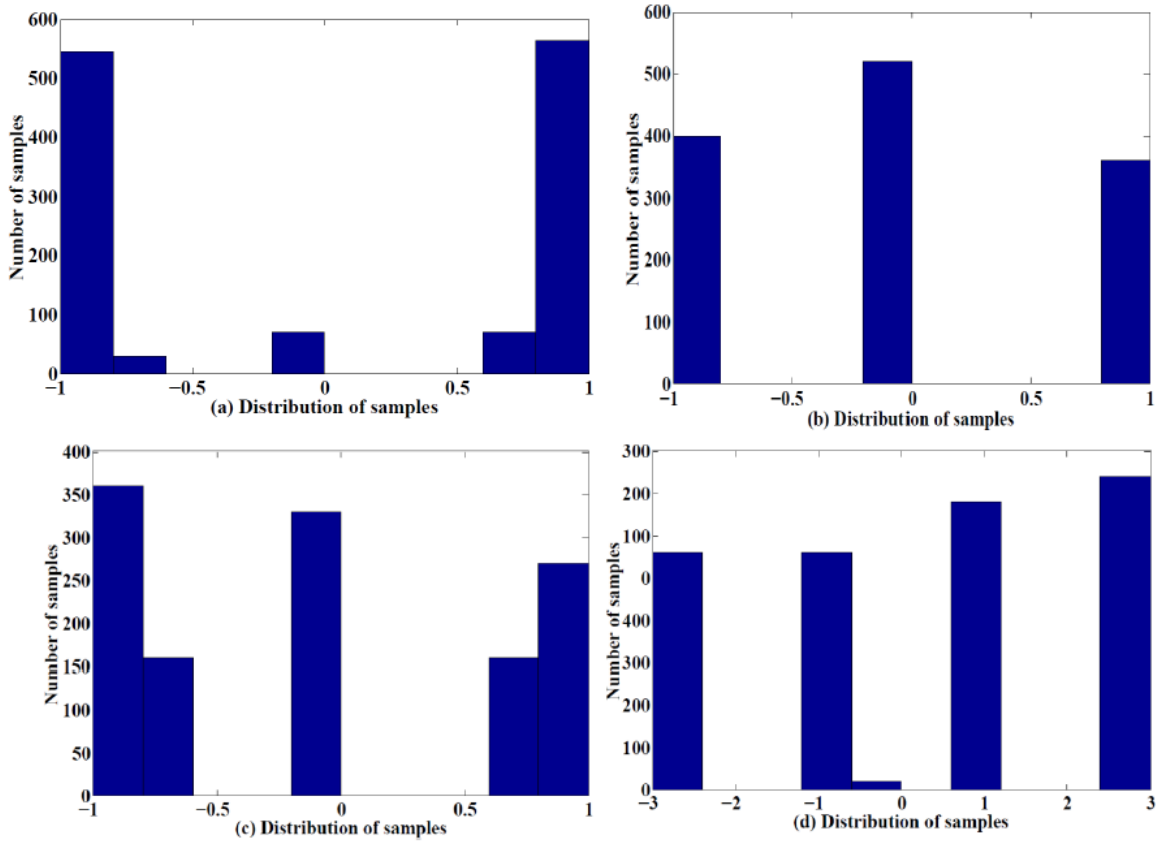

Figure 3.9: Histogram plot for different modulation after digitization, (a).BPSK, (b).QPSK, (c).16-PSK, (d).16-QAM

algorithms such as CWT based algorithm, CFD based algorithm and some others published work. The performance is measured based on probability of correct classification (PCC) and classification rate over 10000 iterations with no pulse shaping filter used at transmitter. PCC is defined as:

$$PCC = \frac{P(BPSK \mid BPSK) + P(QPSK \mid QPSK)}{2}, \tag{3.9}$$

for the case when signal is transmitted with BPSK and QPSK modulation scheme. Received signal is assumed to be contaminated due to AWGN channel. Further, performance of modulation classifier is also tested in Rayleigh fading channel.

Fig. 3.13 shows the comparison of performance of modulation classifier with different modulation schemes. In this case no pulse shaping filter is used. It can be observed from the figure that QPSK performs better than other modulations schemes from low SNRs to high SNRs. Even at very low SNRs, algorithm gives very good accuracy with probability of correction of around 0.9 for QPSK modulation. At low SNRs ($<$ 1dB) BPSK gives worse performance. BPSK, 4-PAM, and 16-QAM perform similarly after 1dB SNR. At 7dB SNR, all modulation schemes except 8-PSK reach accuracy level of 100% (PCC= 1). It can be observed from the Fig. 3.13 that this algorithm performs not so quite well at high SNRs for 8-PSK modulation schemes as for

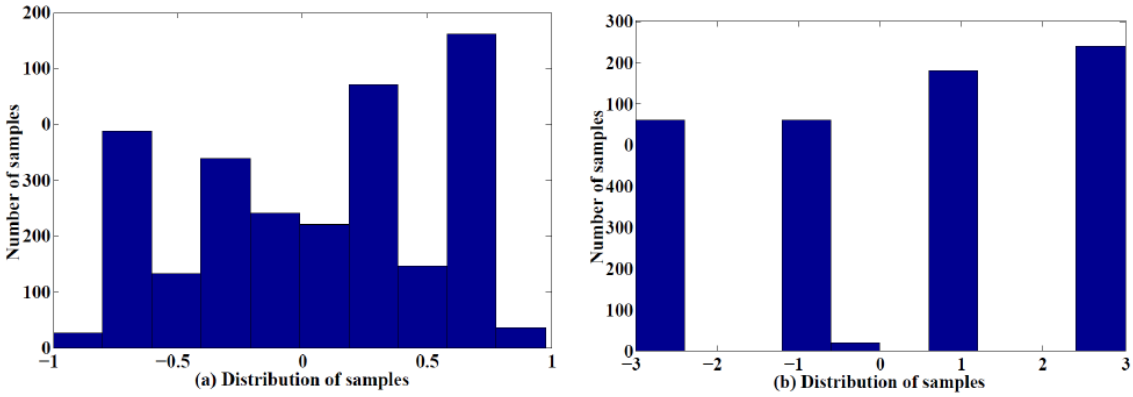

Figure 3.10: Histogram plot for 16-PSK (a).before digitization, (b).after digitization

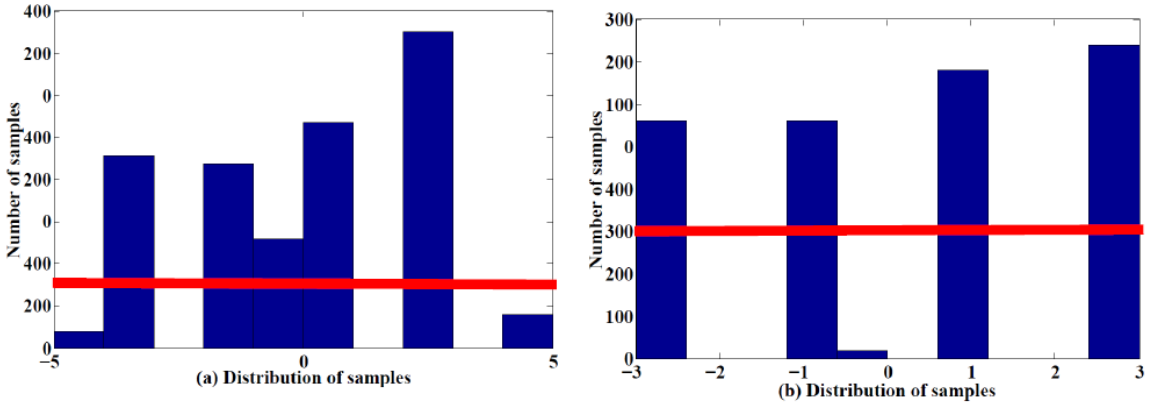

Figure 3.11: Histogram plot for 16-PSK at (a).-2dB, (b).10dB

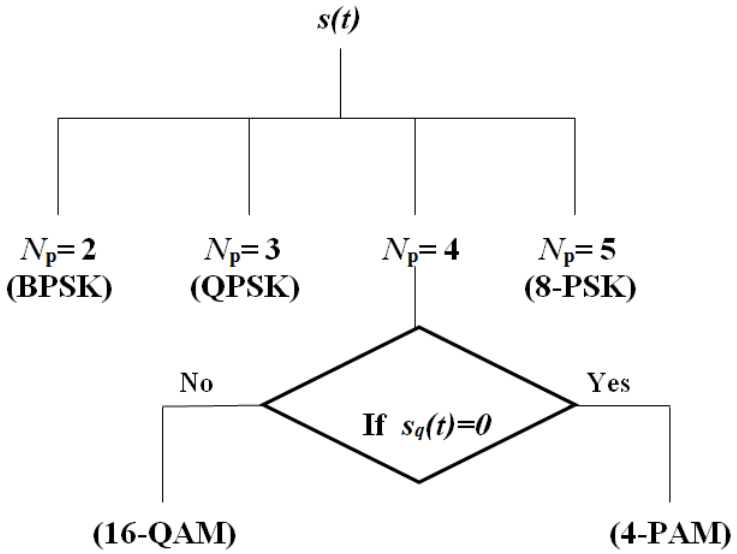

Figure 3.12: Classification tree of modulation classifier

8-PSK the value of PCC is around 0.75. However, from confusion matrix of classifier for different values of SNRs, it can be observed that 8-PSK reaches upto the level of PCC= 0.9 at 15dB SNR. However, it reaches to PCC= 1 at 20dB SNR.

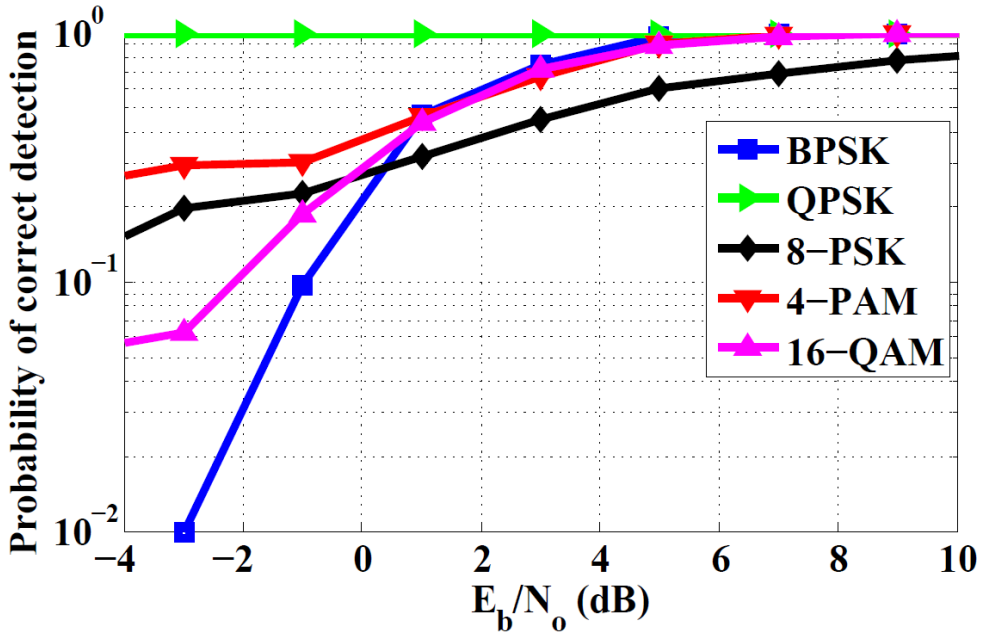

Figure 3.13: Comparison of accuracy of modulation classifier of proposed algorithm for transmitted signal with different modulation schemes and without using any pulse shaping filter

The effect of using pulse shaping filter on proposed algorithm is shown through Fig. 3.14. Gain of pulse shaping filter can change the magnitude and phase of modulated signal due to convolution. In this figure, the performance of classifier is tested for transmitted signal with BPSK, QPSK, 8-PSK, 16-PSK, and 16-QAM modulated schemes. Unlike Fig. 3.13, accuracy level of QPSK is much effected due to filter as it posses PCC= 0.4 at 2dB SNR and the accuracy level of QPSK can reach to 100% at 8dB SNR. In this case, 16-QAM performs better than other modulation schemes as it reaches to 100% accuracy level at 5dB SNR. Like Fig. 3.14, the performance of classifier is worse in BPSK case as it has PCC close to 0.1 at 2dB. However, at 8dB SNR modulation schemes reaches the accuracy level of 100%.

From Fig. 3.15, it can be observed that performance of classifier is not much effected with increase in number of symbols transmitted. At low SNRs ($<$ 4dB), there can be gap of 2dB-4dB SNR in the performance of BPSK modulated signal with increase in number of symbols transmitted. However, similar performance is given by all number of symbols at high SNRs as all have 100% accuracy after 5dB SNR.

Table 3.2 compares the performance of proposed algorithm with HWT algorithm [42] with transmitted signal with 16-QAM modulation scheme. At high SNRs the performance is similar in both cases which is clear from Table. 3.2. However, Fig. 3.16 plots the comparison of performance of proposed algorithm with Wavelet domain features and S-transform domain features in terms of PCC of classifier. It is clear from figure that proposed algorithm perform better

Table 3.1: Confusion matrix of proposed algorithm at different SNRs

SNR		BPSK	QPSK	8-PSK	4-PAM	16-QAM
0dB	BPSK	0.4	0.54	0	0	0.06
	QPSK	0	0.99	0	0	0.01
	8-PSK	0	0.04	0.63	0	0.33
	4-PAM	0	0	0.855	0.145	0
	16-QAM	0	0	0.43	0	0.57
5dB	BPSK	0.97	0.03	0	0	0
	QPSK	0	1	0	0	0
	8-PSK	0	0	0.7	0	0.3
	4-PAM	0	0	0.135	0.865	0
	16-QAM	0	0	0.005	0	0.995
10dB	BPSK	1	0	0	0	0
	QPSK	0	1	0	0	0
	8-PSK	0	0	0.885	0	0.1150
	4-PAM	0	0	0	1	0
	16-QAM	0	0	0	0	1
15dB	BPSK	1	0	0	0	0
	QPSK	0	1	0	0	0
	8-PSK	0	0	0.9	0	0.1
	4-PAM	0	0	0	1	0
	16-QAM	0	0	0	0	1
20dB	BPSK	1	0	0	0	0
	QPSK	0	1	0	0	0
	8-PSK	0	0	1	0	0
	4-PAM	0	0	0	1	0
	16-QAM	0	0	0	0	1

than both algorithms at all SNRs. At 2dB SNR, proposed algorithm has PCC= 0.6 while Wavelet based algorithm has PCC= 0.3 and S-transform based has PCC= 0.25. Hence, proposed algorithm performs much better than both algorithms at low SNRs. The differences in performance decreases with SNR and at 15dB SNR both proposed algorithm and S-transform perform similarly as both reach the accuracy level of 98% - 100%.

In Fig. 3.17, the performance of different estimators (Naive-Bayes [43], SVM [43], GP-KNN [44]) are compared with proposed algorithm in terms of classification rate (ACR). At low SNRs ($<$ 5dB), the performance is poor as compare to other algorithms but after 5dB SNR the performance of proposed algorithm is similar to others. The proposed algorithm can attain the

Table 3.2: Comparision table for proposed algorithm and HWT based algorithm for 16-QAM modulation

SNR (dB)	Classification Rate (%)	
	Proposed	HWT
8	97.2	99.7
10	100	99.4
12	100	100
15	100	100

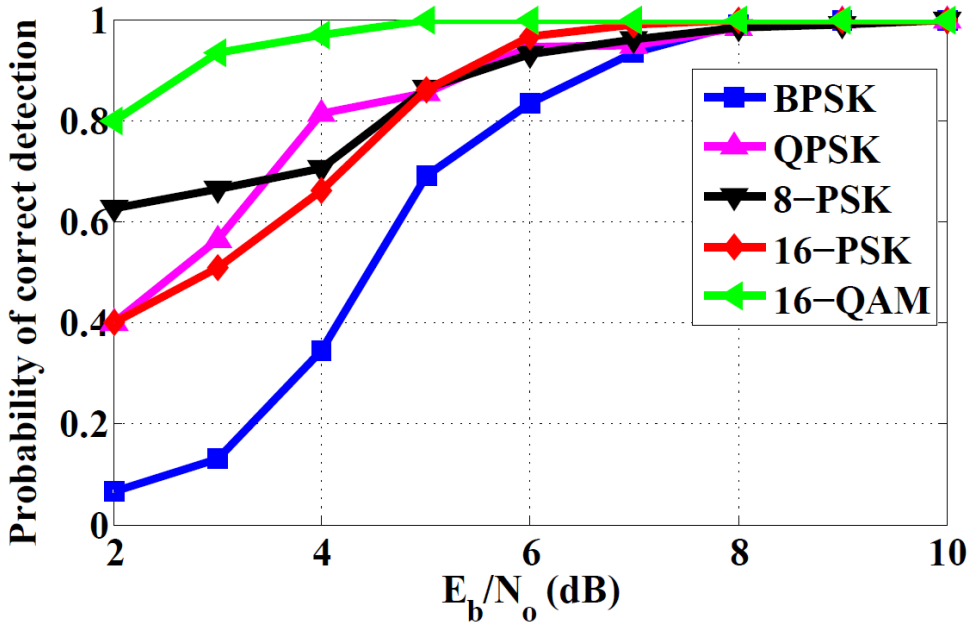

Figure 3.14: Comparison of accuracy of modulation classifier of proposed algorithm for transmitted signal with different modulation schemes using pulse shaping filter with roll-off factor= 0.3

Table 3.3: Comparison table of proposed algorithm with Cyclostationary based algorithm using confusion matrix at 10dB SNR.

	Cyclostationary				**Proposed Algo**			
	BPSK	**16-QAM**	**4-PAM**	**8-PSK**	**BPSK**	**16-QAM**	**4-PAM**	**8-PSK**
BPSK	**0.996**	**0.007**	**-**	**-**	**1**	**0**	**0**	**0**
16-QAM	**-**	**1**	**-**	**-**	**0**	**1**	**0**	**0**
4-PAM	**-**	**0.002**	**0.995**	**0.003**	**0**	**0**	**1**	**0**
8-PSK	**-**	**-**	**-**	**1**	**0**	**0.115**	**0**	**0.885**

accuracy level of 100% at 13 dB SNR which is not achievable by any other mentioned algorithm. 100% accuracy is not archived by other mentioned algorithms even upto 15dB SNR.

Performance of proposed algorithm is compared with cyclostationary based modulation classifier [45] using confusion matrix at 10dB SNR in Table. 3.3. It can be observed from the table that proposed algorithm performs better in terms of BPSK and 4-QAM as 100% accuracy is achieved by these two algorithm while in cyclostationary based algorithm BPSK has PCC= 0.996 and 4-PAM has PCC= 0.995. If we neglect the hardware complexity of symbol rate estimation part of our proposed algorithm and assume that symbol rate is known, then the complexity of our proposed algorithm is significantly less than cyclostationary based algorithm. For 16-QAM modulation performance in both algorithm are similar.

In Fig. 3.18, the performance of different modulation schemes (BPSK, QPSK, 8-PSK, 16-QAM) are compared in multi-path Rayleigh channel. It is obvious that the performance of modulation classifier will degrade due to multi-path effect, which can also be observed from Fig. 3.19. Fig. 3.19 plots the performance of classifier with transmitted signal with BPSK modulation in AWGN

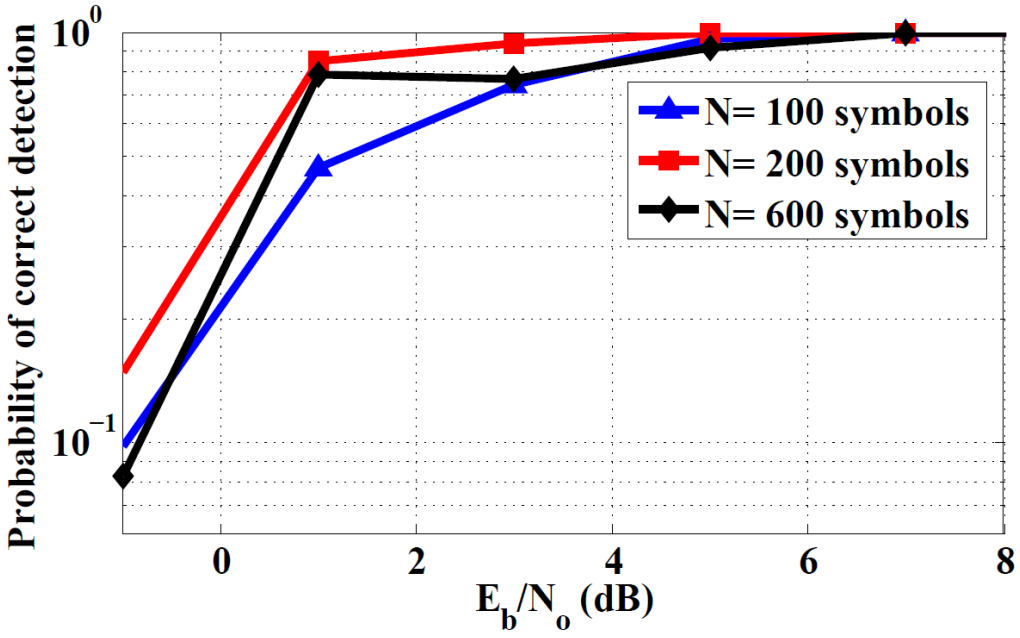

Figure 3.15: Comparison of classification accuracy of proposed estimator for transmitted signal in AWGN with BPSK modulation with no pulse shaping filter being used

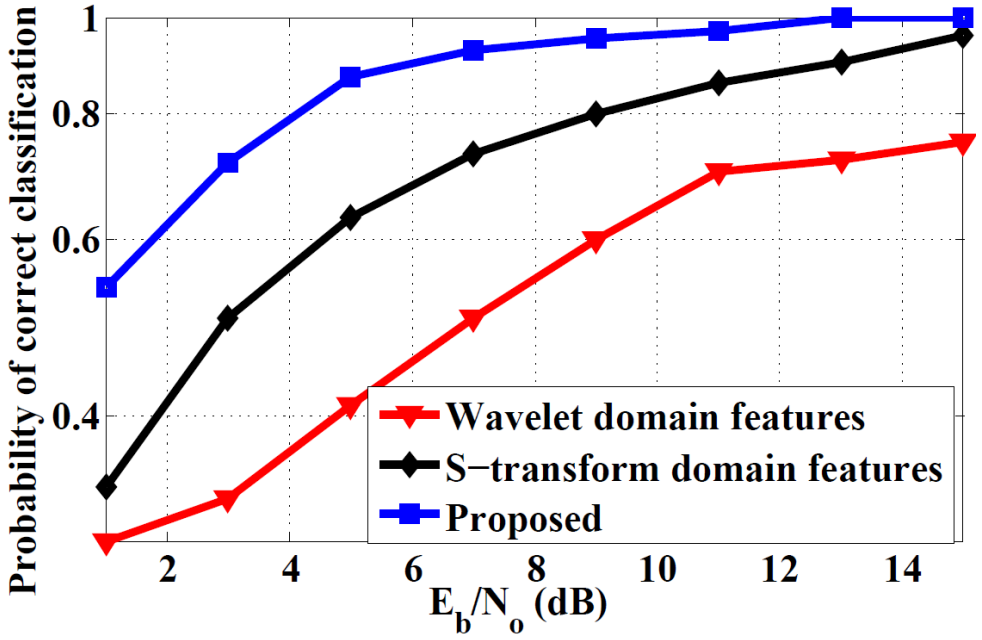

Figure 3.16: Comparison of classification accuracy of proposed classifier with other different classifiers

and Rayleigh fading channel. Due to multi-path effect BPSK modulation reach 100% accuracy at 15dB SNR. However, from Fig. 3.18 it is clear that the nature of the performance of modulation classifier is same as it is in AWGN. Here also QPSK performs better than above mentioned scheme and it looks like its performance is not affected due to multi-path effect. Its accuracy level is 98% to 100% after 5dB SNR. Here also BPSK perform worse than other modulation schemes mentioned above. AT 20dB SNR, all modulation schemes reach 100% accuracy level.

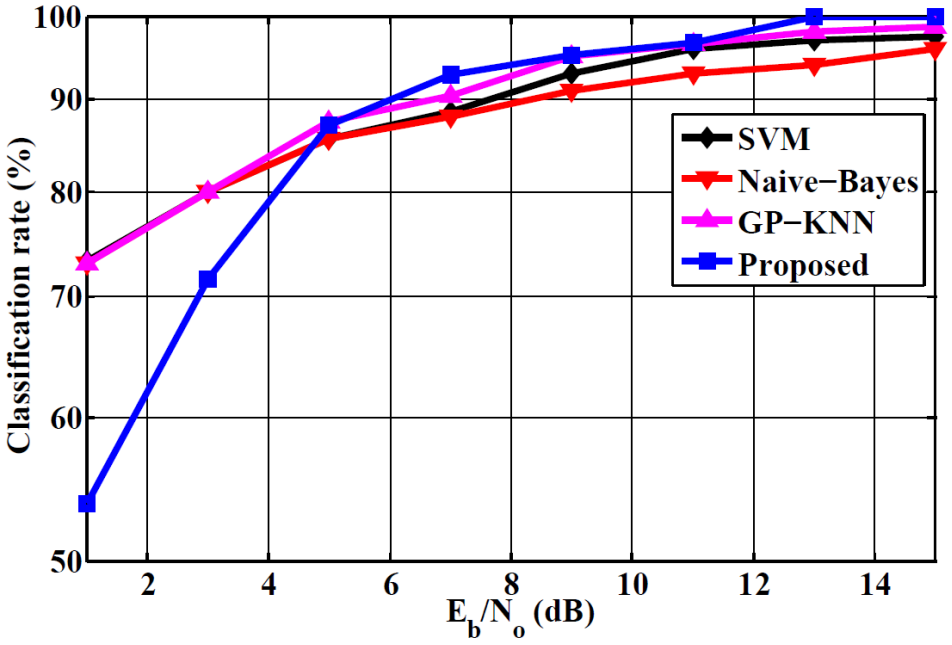

Figure 3.17: Comparison of classification accuracy of proposed classifier with other different classifiers

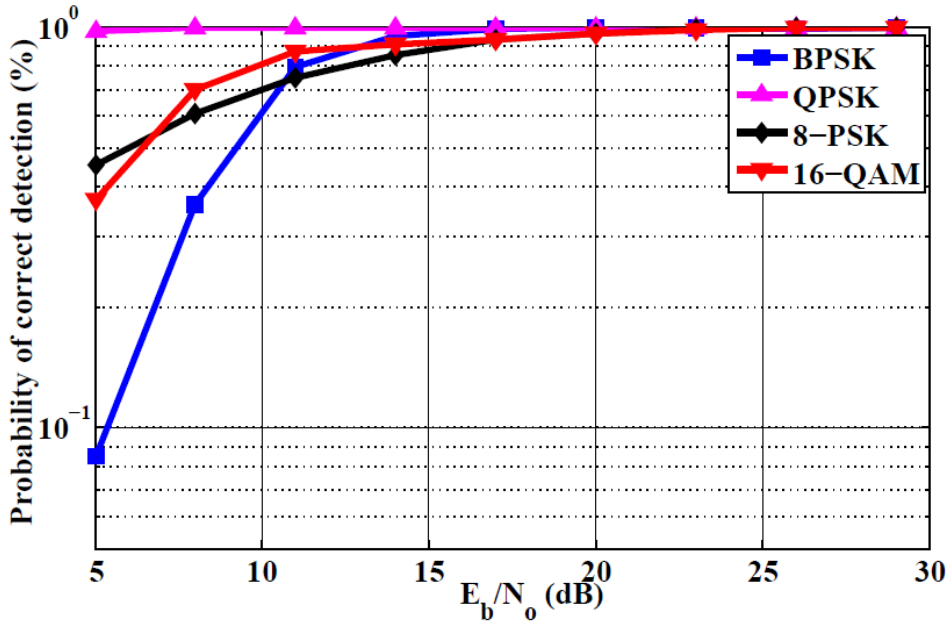

Figure 3.18: Comparison of classification accuracy of proposed classifier with other different modulation schemes

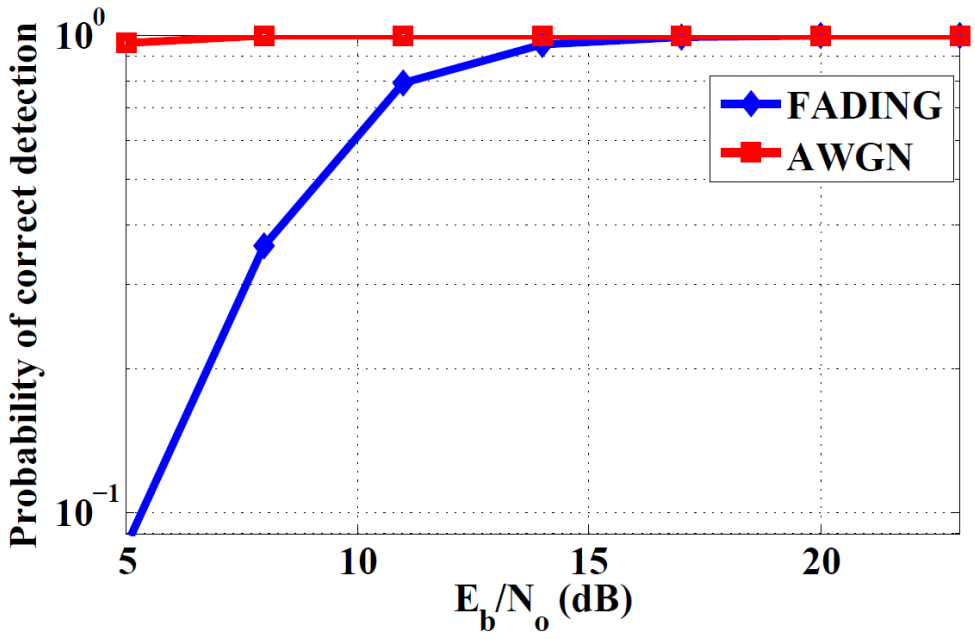

Figure 3.19: Histogram plot for 16-PSK at (a).-2dB, (b).10dB

Chapter 4

Carrier Frequency Estimation

4.1 Introduction

In this chapter, a new carrier frequency estimator for BPSK and PAM modulation schemes are proposed. In this algorithm, all the stages are same which are used in chapter 2, excluding denoising stage. In this case all the operations are done on pass-band signal, thus denoising is not used here, as denoising stage removes high frequency signal coefficient considering them as noise.

The motivation behind carrier frequency estimation is basically when there is a relative motion between transmitter and receiver in communication system. However, one way to do this is by using data aided (DA), where some known training symbols are transmitted periodically [46]. This approach reduces efficiency of transmission rate and may not be feasible in military interception. To solve this problem, some non-data aided (NDA) algorithm is proposed in [47] which do not need training symbols. However, it still requires prior knowledge of some parameters like modulation type. In [7], carrier frequency of linearly modulated signal are estimated using the property of cyclostationarity. This method does not need prior knowledge of any parameters. Based on the phase of auto-correlation of received signal, a carrier frequency estimator is proposed in [48] which is complete blind. However its performance get worse at low SNRs. To remove this problem a fast algorithm to estimate carrier frequency is proposed in [49].

In this chapter, a carrier frequency estimator is proposed which exploits the property of cyclostationary in wavelet domain. The proposed algorithm is completely blind which do not require prior knowledge of any parameters. Simulation results prove the superiority of proposed algorithm over other conventional algorithms, as it performs good at low SNRs.

The remainder of this paper is organized as follows. Section II is devoted to developing the proposed carrier frequency estimation. Section III reports the simulation results.

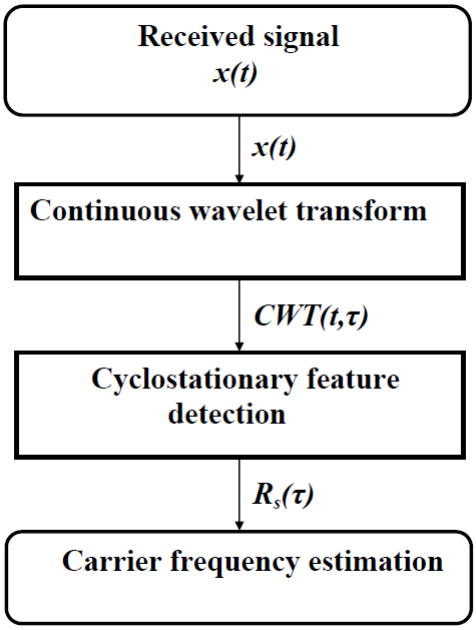

Figure 4.1: Flow diagram of proposed carrier frequency estimator

4.2 Carrier Frequency Estimator

In this section, the proposed carrier frequency estimator is discussed. Unlike symbol rate estimator, the carrier frequency estimation can be categorized into two stages , i.e. 1) CWT and 2) Cyclostationary feature detection (CFD), as shown in Fig. 4.1. In the first stage, received signal is transformed into wavelet domain by applying CWT. Finally, detecting the cyclostationary features of the signal in Wavelet domain, the carrier frequency is estimated.

In the following subsections , the proposed carrier frequency estimator is discussed in detail. In Section 4.A, the signal model is discussed followed by CWT of the received signal in section 4.B. Finally, estimation of carrier frequency using cyclostationary feature detection is presented in section 4.C.

4.2.1 Signal Model

The down-converted base-band signal at the receiver can be written as

$$x(t) = s(t) + n(t), \tag{4.1}$$

where $s(t)$ is the transmitted signal and $n(t)$ is independent of signal component, represents additive white gaussian noise (AWGN) with mean zero and variance σ_n^2. In this chapter, presence of pulse shaping filter at transmitter is not taken into account. However in chapter 3, performance is analyzed by considering the effect of pulse shaping filter. An BPSK signal $s(t)$

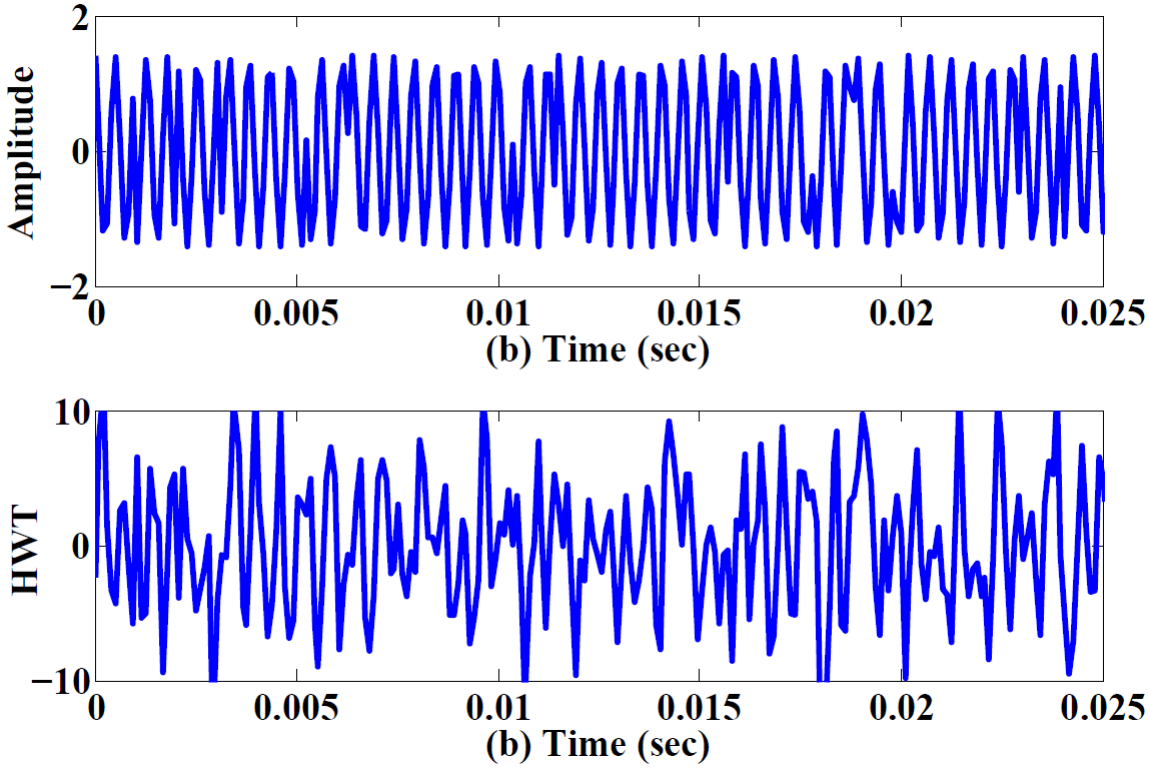

Figure 4.2: (a).Received BPSK signal, (b).Plot of CWT of the received denoised signal at SNR= 2dB

can be written as

$$s(t) = A(t)e^{(w_c t + \theta c + \emptyset(t))}, \tag{4.2}$$

where

$$\emptyset(t) = \sum_{i=1}^{N} \alpha_i \Pi(t - iT_s), \tag{4.3}$$

$$\alpha_i \in \{0, \pi\},$$

$A(t)$ and $\emptyset(t)$ represent amplitude and phase of the received signal at time t, w_c is carrier frequency and θ_c is the carrier phase. For simplicity θ_c is assumed to be zero. For ease of analysis, we assume that $s(t)$ is a PSK modulated signal hence $A(t) = A$. M represents the number of symbols, T_s is the symbol period, $\Pi(t)$ is the unit pulse function of duration T_s. Finally, $s(t)$ can be written as

$$s(t) = A(t)e^{(w_c t + \emptyset(t))}, \tag{4.4}$$

4.2.2 Wavelet Transform

CWT of received signal will spikes at each phase transitions of received signal. The derivation of CWT is done in [5]. From Fig. 4.2 it can be observed that each phase transition in the received signal leads to spike. From Fig. 4(b) it can be observed that at low SNR (2dB) there are several unwanted spikes because of immense noise power.

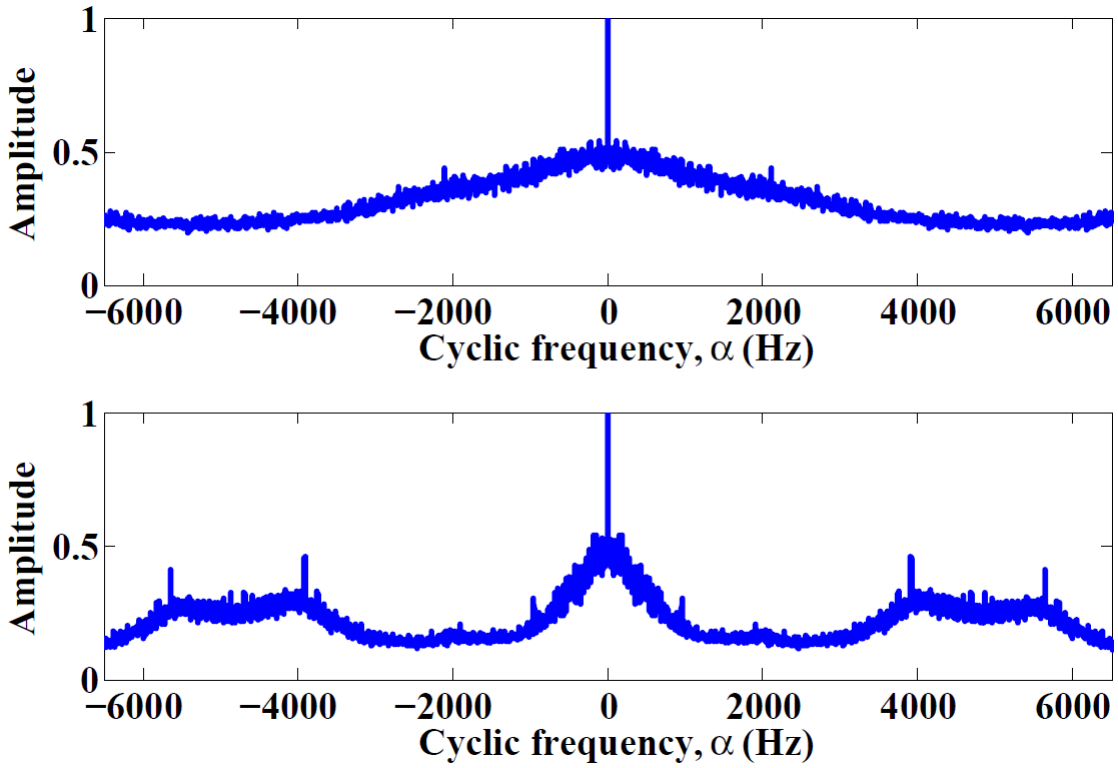

Figure 4.3: Illustration of symbol rate estimation using the proposed algorithm for transmitted carrier frequency of 1955.5 Hz at (a).SNR= -2dB, (b).SNR=8dB

4.2.3 Carrier Frequency Estimation Using Cyclic Autocorrelation

As discussed in chapter 2, since HWT does not transform the phase of PSK signal, it is still a cyclostationary random process. Cyclic statistics preserve phase information. Thus, they can be exploited in estimation of carrier frequency. Hence, complete derivation for PSK signal done in [7], is applicable here. As a result, by choosing some suitable value of lag, τ_{fix}, cyclic autocorrelation ($R_x(\alpha, \tau_{fix})$) will posses non zero values at only cyclic frequency, $\alpha \in \{0, \pm 2w_c\}$. From Fig. 4.3(b) peaks can be observed at cyclic frequency, $\alpha \in \{0, \pm 2w_c\}$. However, Fig. 4.3(a) shows that at very low SNR no peaks occur. Hence, error in estimating carrier frequency is more.

4.3 Simulation Results

In order to evaluate the performance of the proposed algorithm, a linearly modulated signal is assumed to be transmitted. It is also assumed that the carrier frequency estimation is ideal or the receiver has *priori* knowledge of the carrier frequency. To check the performance of estimator, signal with carrier frequency = 1955.5Hz is transmitted. The performance is tested for BPSK, 4-PAM, and 8-PAM modulation scheme. The performance is measured based on percentage error and success rate over 10000 iterations. Percentage error is defined as $|f_s - f_s^{'}| \times 100/f_s$, where f_s and $f_s^{'}$ are carrier frequency and estimated carrier frequency respectively. Received

signal is assumed to be contaminated due to AWGN channel.

Fig. 4.4 plots the performance of carrier frequency estimator for above mentioned modulation schemes. It can be inferred from figure that estimator perform better for 8-PAM and worse for BPSK modulation. For BPSK modulation error is reduced to 0.01% at 10dB SNR. 4-PAM can attain same accuracy at 7dB SNR while for 8-PAM it is 4dB SNR. After attaining percentage error of 0.01% the performance of each modulation schemes saturate. Thus, after 10dB SNR, each modulation schemes perform similarly.

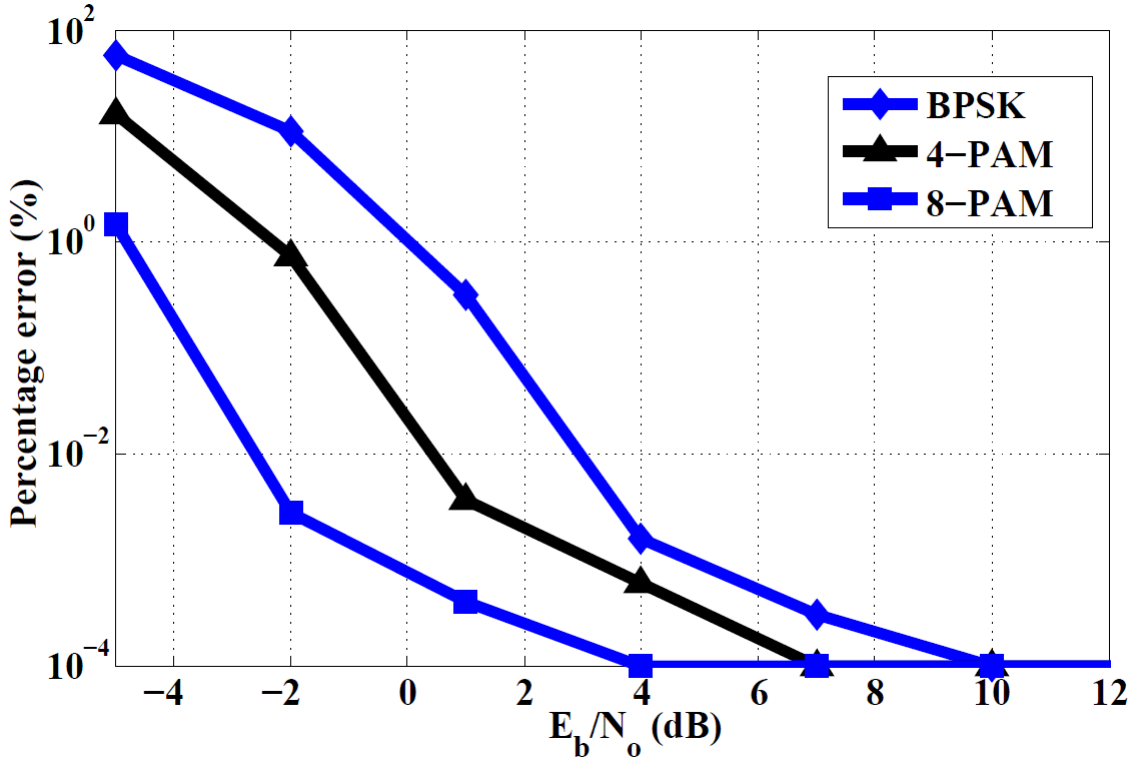

Figure 4.4: Flow diagram of proposed carrier frequency estimator

Chapter 5

Complexity Analysis of Algorithm

In this section, complexity of proposed algorithm in terms of number of gate counts is calculated. To begin with, the number of multipliers, adders and multiplexers required for the proposed algorithm are calculated. The proposed algorithm consists of three stages: 1) Denoising, 2) CWT, and 3) CFD. The total number of adders, multipliers and multiplexers for each stage are given in Table 5.1 where N is the number of received samples. It can be observed that CFD is the most computationally intensive stage in the proposed algorithm.

Next, total gate count requirement of the proposed algorithm is obtained using Table 5.1. To do that, a 16x16 bit multiplier, a 2:1 multiplexer and 32 bit adder were synthesized on a TSMC 0.65nm process. The Synopsys Design Compiler was used to estimate the cell area. The gate count is obtained by normalizing the cell area values by that of a 2:1 NAND gate from the same library. The total gate count in Table 5.2 is the sum of the gate counts of multipliers, adders and multiplexers. Note that total gate count requirements of single multiplier, adder and multiplexer are 1600, 225, and 25 respectively. It can be observed that the gate count requirement of the proposed algorithm is slightly higher than (0.2%) that of CFD based symbol rate detection algorithm. This is the penalty paid to achieve more than 8% (at 0dB SNR) improvement in the symbol rate detection error over both the CFD based algorithm and the CWT based algorithm as shown in Fig. 2.7.

Table 5.1: Calculation of number of adder, multipler and multiplexer of proposed algorithm

Stage	**Adder**	**Multiplier**	**Mux (2:1)**
Denoising	$17N$ - 55	$24N$+15	5
CWT	7	8	4
CFD	$2(3N\text{-}3+(2N\text{-}1)\ log_2(2N\text{-}1))$	$4(2N+\ \frac{(2N-1)^2}{2} log_2(2N\text{-}1))$	0

Table 5.2: Comparision of gate count for each algorithm for N (number of received samples)= 200

Algorithm	**Number of adder**	**Number of multiplier**	**Number of mux (2:1)**	**Gate count**
Proposed algorithm	11441	2757494	9	4414564850
CWT based symbol rate estimator	7	8	4	14475
CFD based symbol rate estimator	8089	2752671	0	4406093625

Chapter 6

Conclusions and Future Works

6.1 Conclusions

In this paper, a new algorithm for accurate estimating the symbol rate, modulation type and carrier frequency of any received signal has been proposed. The proposed algorithm exploits excellent localization property of wavelet transform along with superiority of cyclostationary feature detection in low SNR environment. Simulation and gate count complexity results validate the superiority of the proposed algorithm over others. Simulation results are presented for both AWGN and Fading channels.

The performance of proposed symbol rate estimator is compared with others existing algorithms like CFD based, wavelet based and filter bank based algorithms. Simulation results validate the superiority of proposed algorithm over these algorithms as proposed algorithm performs much better than existing algorithm at low SNRs ($< 3dB$). However, we also paid for it as gate count requirement of the proposed algorithm is slightly higher than (0.2%) that of CFD based algorithm. This is the penalty paid to achieve more than 8% (at 0dB SNR) improvement in the symbol rate detection error over both the CFD based algorithm and the CWT based algorithm. The performance of symbol rate estimator improves with increase in modulation order which is unusual.

The proposed algorithm of symbol rate estimation is further extended to automatic modulation classification (AMC). The modulation classifier is proposed for BPSK, QPSK, 8-PSK, 4-PAM, and 16-QAM modulation schemes. The classifier is feature-based classifier because modulations are differentiated using histogram plot and histogram plot have different features for each modulation schemes. Proposed AMC does not require any training symbols. Simulation results show that the performance of proposed algorithm is better than existing algorithms. The proposed AMC gives 100% accuracy at 13dB SNR.

The proposed algorithm is further extended to carrier frequency estimation of BPSK and PAM modulated signals. In this case all the operations are done on pass-band signal, thus denoising is not used here, as denoising stage removes high frequency signal coefficient considering them

as noise. The proposed algorithm gives good result at low SNRs ($< 2dB$).

6.2 Future Works

- In future the work can be extended to estimate blind parameters under both coherent and non-coherent cases. Under coherent case carrier phase is known but in case of non-coherent case carrier phase is not known.
- Future works include extension of the proposed algorithm for bandwidth of any received signal and efficient implementation of the proposed algorithm on FPGA using partial reconfiguration approach for validation using real radio signals.
- The work can be extended to encryption, decryption and demodulation of data as decryption and demodulation of data requires knowledge of modulation type of transmitted signal.
- Work can be done to estimate carrier frequency for more number of modulation schemes in both AWGN and Rayleigh channel. Even work can be extended to other fading channels like Rician fading, Nakagami fading, ECG fading.

Bibliography

[1] Q. Li, S. H. Ting, A. Pandharipande, and Y. Han, "Cognitive spectrum sharing with two-way relaying systems," *IEEE Transactions on Vehicular Technology*, vol. 60, no. 3, pp. 1233–1240, 2011.

[2] S. Majhi and T. S. Ho, "Blind symbol-rate estimation and test bed implementation of linearly modulated signals," *IEEE Transactions on Vehicular Technology*, vol. 64, no. 3, pp. 954–963, 2015.

[3] K. Ho, W. Prokopiw, and Y. Chan, "Modulation identification of digital signals by the wavelet transform," *IEE Proceedings-Radar, Sonar and Navigation*, vol. 147, no. 4, pp. 169–176, August 2000.

[4] M. Frisch and H. Messer, "The use of the wavelet transform in the detection of an unknown transient signal," *IEEE Transactions on Information Theory,*, vol. 38, no. 2, pp. 892–897, March 1992.

[5] Y. T. Chan, J. W. Plews, and K. C. Ho, "Symbol rate estimation by the wavelet transform," in *IEEE International Symposium on Circuits and Systems*, vol. 1, pp. 177–180, June 1997.

[6] X. Jun, W. Fu-ping, and W. Zan-ji, "The improvement of symbol rate estimation by the wavelet transform," in *International Conference on Communications, Circuits and Systems*, vol. 1, pp. 100–103, Hong Kong, China, May 2005.

[7] Y. Jin and H. Ji, "Cyclic autocorrelation based blind parameter estimation of psk signals," in *6th International Conference on ITS Telecommunications*, pp. 1293–1296, Chengdu, China, June 2006.

[8] G. Sun, J. An, J. Yang, Y. Jing, and Z. Li, "Symbol rate estimation using cyclic correlation and haar wavelet transform," in *IEEE 4th International Conference on Wireless Communications, Networking and Mobile Computing*, pp. 1–4, Dalian, China, October 2008.

[9] Y. Liang, Y. Yao, T. Dai, and M. Qin, "A blind symbol rate estimation of weak signal based on cyclic spectrum and wavelet transform," *Journal of Information & Computational Science*, pp. 1917–1924, October 2012.

[10] Z. Yu, Y. Q. Shi, and W. Su, "Symbol-rate estimation based on filter bank," in *IEEE International Symposium on Circuits and Systems*, vol. 2, pp. 1437–1440, May 2005.

[11] P. Ciblat, P. Loubaton, E. Serpedin, and G. B. Giannakis, "Asymptotic analysis of blind cyclic correlation-based symbol-rate estimators," *IEEE Transactions on Information Theory*, vol. 48, no. 7, pp. 1922–1934, Jul 2002.

[12] S. Majhi and T. S. Ho, "Blind symbol-rate estimation and test bed implementation of linearly modulated signals," *IEEE Transactions on Vehicular Technology*, vol. 64, no. 3, pp. 954–963, March 2015.

[13] X. Li, Q. Han, Z. Liu, and Z. Wu, "Novel modulation detection scheme for underwater acoustic communication signal through short-time detailed cyclostationary features," in *2014 IEEE Wireless Communications and Networking Conference (WCNC)*, April 2014, pp. 624–629.

[14] Z. Wu and T. C. Yang, "Blind cyclostationary carrier frequency and symbol rate estimation for underwater acoustic communication," in *2012 IEEE International Conference on Communications (ICC)*, June 2012, pp. 3482–3486.

[15] D. Li, J. Ellinger, Z. Liu, Z. Wu, and Z. Zhang, "Mixed signal detection and symbol rate estimation based on spectral coherent features," in *Military Communications Conference, MILCOM 2015 - 2015 IEEE*, Oct 2015, pp. 263–268.

[16] S. A. Mahmoud and E. A. Soliman, "Multi-standard receiver baseband chain using digitally programmable ota based on ccii and current division networks," *Journal of Circuits, Systems, and Computers*, vol. 22, no. 04, pp. 1–5, October 2013.

[17] S. Narasimhan, N. Basumallick, and S. Veena, "Introduction to wavelet transform: a signal processing approach. alpha science international ltd," 2012.

[18] P. M. Grant, A. R. Mirzai, K. E. Brown, and T. M. Crawford, "Intelligent techniques for electronic component and system alignment," *Electronics Communication Engineering Journal*, vol. 1, no. 1, pp. 23–32, Jan 1989.

[19] M. K. K. Rao, S. K. PV, and B. Sellappan, "Embedded tutorial et2: Digital subscriber line," in *2012 25th International Conference on VLSI Design*, Jan 2012, pp. 33–34.

[20] "Broadcast digital subscriber lines," *IEEE Journal on Selected Areas in Communications*, vol. 13, no. 9, pp. 1550–1557, Dec 1995.

[21] S. G. Maghrebi, M. Lotfizad, and M. Ghanbari, "The better performance of the new non-rectangular qam with fht in adsl system based on dmt without cyclic prefix," in *2007 15th International Conference on Digital Signal Processing*, July 2007, pp. 335–338.

[22] Y. Zhang, N. Ansari, and W. Su, "Optimal decision fusion based automatic modulation classification by using wireless sensor networks in multipath fading channel," in *Global Telecommunications Conference (GLOBECOM 2011), 2011 IEEE*, Dec 2011, pp. 1–5.

[23] L. Haring, Y. Chen, and A. Czylwik, "Efficient modulation classification for adaptive wireless ofdm systems in tdd mode," in *2010 IEEE Wireless Communication and Networking Conference*, April 2010, pp. 1–6.

[24] F. Zorzi, L. Mucchi, L. S. Ronga, P. Marcocci, E. D. Re, and M. Luise, "Non coherent demodulation of bpsk secure symbols," in *Wireless Personal Multimedia Communications (WPMC), 2013 16th International Symposium on*, June 2013, pp. 1–6.

[25] M. M. Khairy and E. Geraniotis, "Symbol aided and pilot aided demodulation and its performance improvement using iterative decoding for fading channels," in *Personal, Indoor and Mobile Radio Communications, 2000. PIMRC 2000. The 11th IEEE International Symposium on*, vol. 1, 2000, pp. 158–165 vol.1.

[26] B. Ramkumar, "Automatic modulation classication and blind equalization for cognitive radios," 2011.

[27] K. E. Nolan, L. Doyle, P. Mackenzie, and D. OMahony, "Modulation scheme classification for 4g software radio wireless networks," in *Proc. IASTED*, 2002, pp. 4–10.

[28] O. Ozdemir, R. Li, and P. K. Varshney, "Hybrid maximum likelihood modulation classification using multiple radios," *IEEE Communications Letters*, vol. 17, no. 10, pp. 1889–1892, October 2013.

[29] A. Ramezani-Kebrya, I. M. Kim, D. I. Kim, F. Chan, and R. Inkol, "Likelihood-based modulation classification for multiple-antenna receiver," *IEEE Transactions on Communications*, vol. 61, no. 9, pp. 3816–3829, September 2013.

[30] T. Wimalajeewa, J. Jagannath, P. K. Varshney, A. Drozd, and W. Su, "Distributed asynchronous modulation classification based on hybrid maximum likelihood approach," in *Military Communications Conference, MILCOM 2015 - 2015 IEEE*, Oct 2015, pp. 1519–1523.

[31] J. A. Sills, "Maximum-likelihood modulation classification for psk/qam," in *Military Communications Conference Proceedings, 1999. MILCOM 1999. IEEE*, vol. 1, 1999, pp. 217–220 vol.1.

[32] W. Wei and J. M. Mendel, "A new maximum-likelihood method for modulation classification," in *Signals, Systems and Computers, 1995. 1995 Conference Record of the Twenty-Ninth Asilomar Conference on*, vol. 2, Oct 1995, pp. 1132–1136 vol.2.

[33] ——, "Maximum-likelihood classification for digital amplitude-phase modulations," *IEEE Transactions on Communications*, vol. 48, no. 2, pp. 189–193, Feb 2000.

[34] A. A. Tadaion, M. Derakhtian, S. Gazor, and M. R. Aref, "Likelihood ratio tests for psk modulation classification in unknown noise environment," in *Canadian Conference on Electrical and Computer Engineering, 2005.*, May 2005, pp. 151–154.

[35] C. Yin, B. Li, and Y. Li, "Modulation classification of mqam signals from their constellation using clustering," in *Communication Software and Networks, 2010. ICCSN '10. Second International Conference on*, Feb 2010, pp. 303–306.

[36] A. Kubankova and D. Kubanek, "Algorithms of digital modulation classification and their verification," *WSEAS Transactions on Communications*, vol. 9, no. 9, pp. 563–572, 2010.

[37] M. Harbaji, K. Shaban, and A. El-Hag, "Classification of common partial discharge types in oil-paper insulation system using acoustic signals," *IEEE Transactions on Dielectrics and Electrical Insulation*, vol. 22, no. 3, pp. 1674–1683, 2015.

[38] A. Swedan, A. El-Hag, and K. Assaleh, "Acoustic detection of partial discharge using signal processing and pattern recognition techniques," *Insight-Non-Destructive Testing and Condition Monitoring*, vol. 54, no. 12, pp. 667–672, 2012.

[39] C. Yin, B. Li, and Y. Li, "Modulation classification of mqam signals from their constellation using clustering," in *Communication Software and Networks, 2010. ICCSN'10. Second International Conference on.* IEEE, 2010, pp. 303–306.

[40] N. P. Geisinger, "Classification of digital modulation schemes using linear and nonlinear classifiers," Ph.D. dissertation, Monterey, California. Naval Postgraduate School, 2010.

[41] N. An, B. Li, and M. Huang, "Modulation classification of higher order mqam signals using mixed-order moments and fisher criterion," in *Computer and Automation Engineering (ICCAE), 2010 The 2nd International Conference on*, vol. 3. IEEE, 2010, pp. 150–153.

[42] L. Hong, "Low-complexity identifier for m-ary qam signals," in *IEEE Southeastcon 2009.* IEEE, 2009, pp. 164–168.

[43] L. Qian and C. Zhu, "Modulation classification based on cyclic spectral features and neural network," in *Image and Signal Processing (CISP), 2010 3rd International Congress on*, vol. 8. IEEE, 2010, pp. 3601–3605.

[44] A. Güner and I. Kaya, "Periodic variation method for blind symbol rate estimation," *International Journal of Communication Systems*, vol. 27, no. 12, pp. 4199–4209, 2014.

[45] B. Ramkumar, "Automatic modulation classification for cognitive radios using cyclic feature detection," *IEEE Circuits and Systems Magazine*, vol. 9, no. 2, pp. 27–45, 2009.

[46] M. Morelli, U. Mengali, and G. M. Vitetta, "Further results in carrier frequency estimation for transmissions over flat fading channels," *IEEE communications Letters*, vol. 2, no. 12, pp. 327–330, 1998.

[47] N. K. Jablon, "Joint blind equalization, carrier recovery and timing recovery for high-order qam signal constellations," *IEEE Transactions on signal processing*, vol. 40, no. 6, pp. 1383–1398, 1992.

[48] Z. Yu, Y. Q. Shi, and W. Su, "A blind carrier frequency estimation algorithm for digitally modulated signals," in *Military Communications Conference, 2004. MILCOM 2004. 2004 IEEE*, vol. 1. IEEE, 2004, pp. 48–53.

[49] S. Kay, "A fast and accurate single frequency estimator," *IEEE Transactions on Acoustics, Speech, and Signal Processing*, vol. 37, no. 12, pp. 1987–1990, 1989.

Appendix

Appendix A

In this appendix, the performance of symbol rate estimator for BPSK and 16-QAM modulation schemes are compared, when deterministic data are taken in such a way that in a window of same length, both modulation schemes can possess same number of symbol transitions. However, I-component of transmitted signal possess less number of symbol transitions when compared with I-component of BPSK signal (as shown in Fig. 6.1). Hence the number of spikes are less in case of 16-QAM modulation which is clear from Fig. 6.2. Unlike in case of random signal, from Fig. 6.3 it can be observed that in case of deterministic signal BPSK performs much better than 16-QAM for any value of SNRs between -5dB SNR to 11dB SNR.

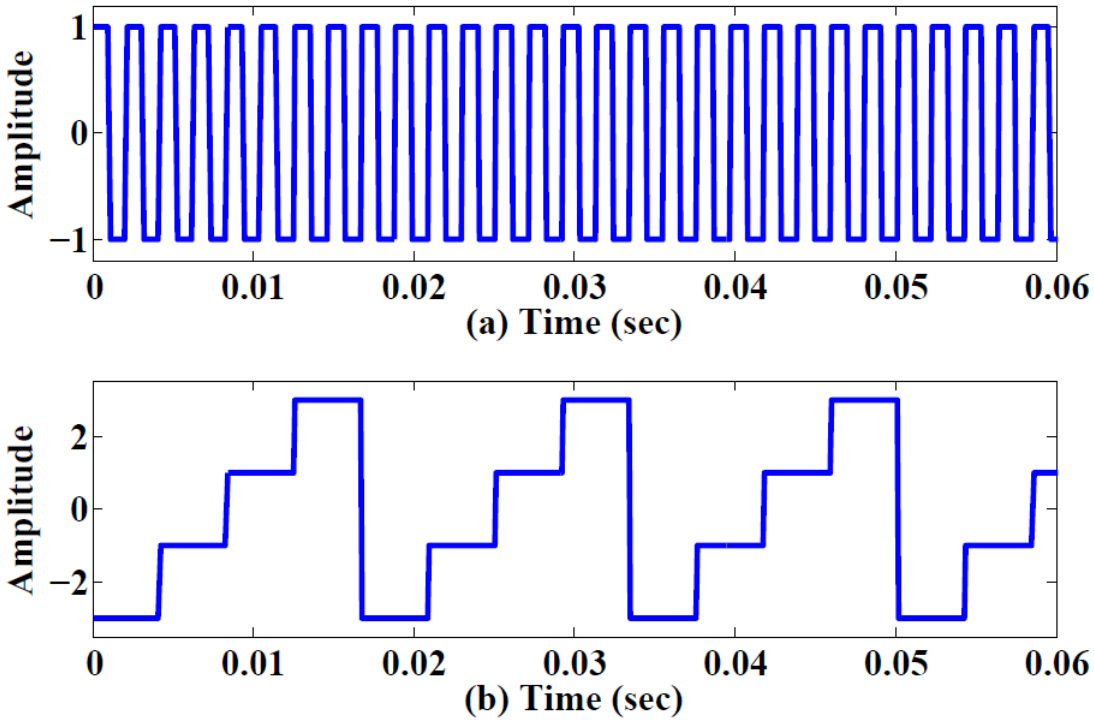

Figure 6.1: (a).I-component of the transmitted BPSK signal, (b) I-component of the transmitted 16-QAM signal, when rate of symbol transition is same in transmitted signal.

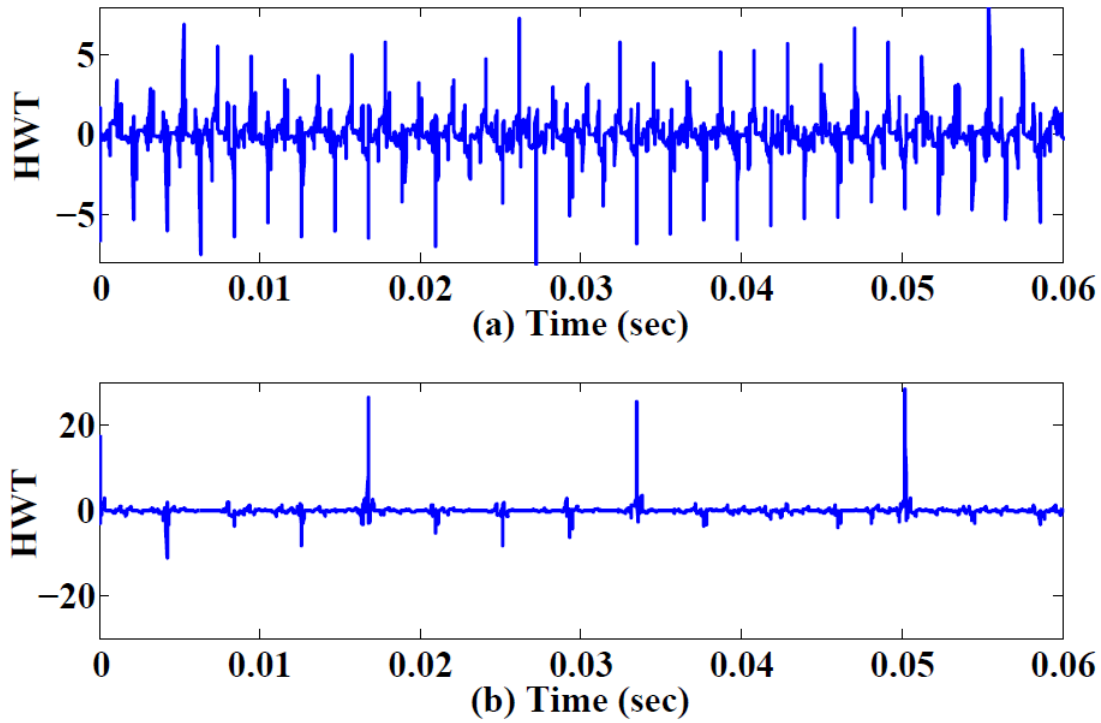

Figure 6.2: (a).Plot of *cwt* of the received denoised signal with BPSK modulation, (b).Plot of *cwt* of the received denoised signal with 16-QAM modulation

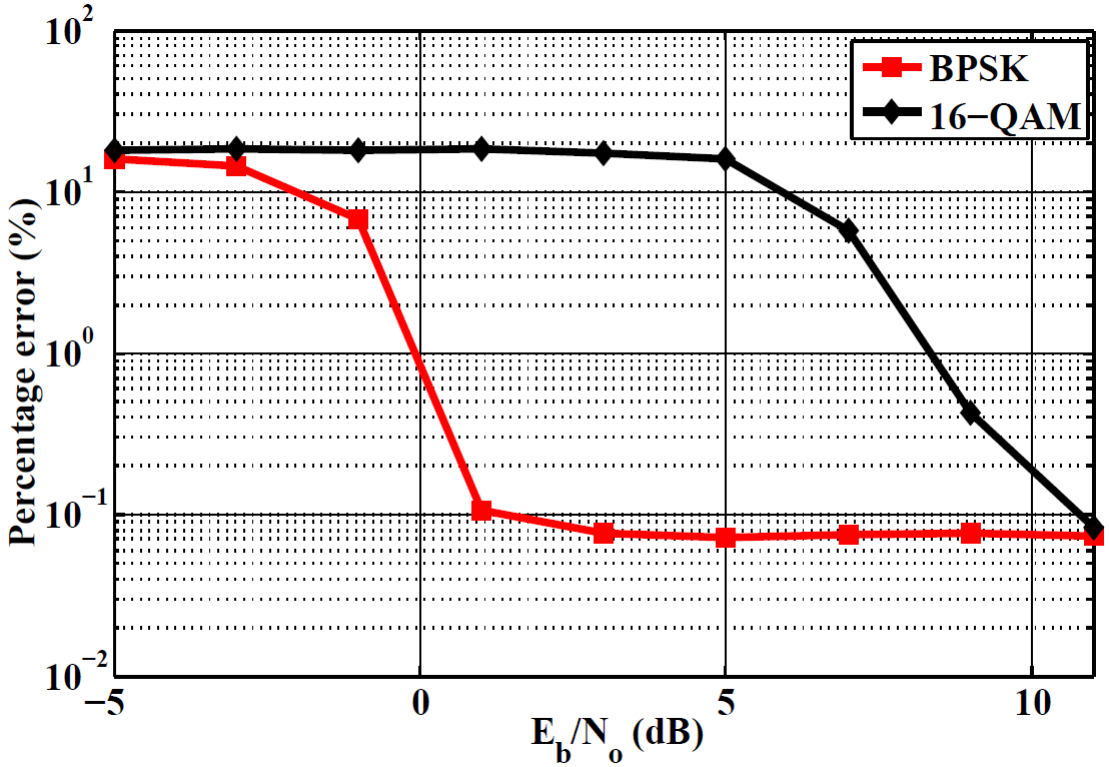

Figure 6.3: Comparison of the performance of symbol rate estimator with BPSK and 16-QAM modulation in case of deterministic signal